

การสังเคราะห์อนุภาคระดับนาโนเมตรของเพอราริน-ทองคำสำหรับการนำส่งทางผิวหนัง



บทคัดย่อและแฟ้มข้อมูลฉบับเต็มของวิทยานิพนธ์ตั้งแต่ปีการศึกษา 2554 ที่ให้บริการในคลังปัญญาจุฬาฯ (CUIR)  
เป็นแฟ้มข้อมูลของนิสิตเจ้าของวิทยานิพนธ์ ที่ส่งผ่านทางบัณฑิตวิทยาลัย

The abstract and full text of theses from the academic year 2011 in Chulalongkorn University Intellectual Repository (CUIR)  
are the thesis authors' files submitted through the University Graduate School.

วิทยานิพนธ์นี้เป็นส่วนหนึ่งของการศึกษาตามหลักสูตรปริญญาวิทยาศาสตรมหาบัณฑิต  
สาขาวิชาปิโตรเคมีและวิทยาศาสตร์พอลิเมอร์  
คณะวิทยาศาสตร์ จุฬาลงกรณ์มหาวิทยาลัย  
ปีการศึกษา 2560  
ลิขสิทธิ์ของจุฬาลงกรณ์มหาวิทยาลัย

SYNTHESIS OF PUERARIN-GOLD NANOPARTICLES FOR TRANSDERMAL DELIVERY



A Thesis Submitted in Partial Fulfillment of the Requirements  
for the Degree of Master of Science Program in Petrochemistry and Polymer Science

Faculty of Science

Chulalongkorn University

Academic Year 2017

Copyright of Chulalongkorn University

Thesis Title	SYNTHESIS OF PUERARIN-GOLD NANOPARTICLES FOR TRANSDERMAL DELIVERY
By	Miss Kwanruen Chanpeng
Field of Study	Petrochemistry and Polymer Science
Thesis Advisor	Professor Nongnuj Muangsin, Ph.D.

---

Accepted by the Faculty of Science, Chulalongkorn University in Partial  
Fulfillment of the Requirements for the Master's Degree

.....Dean of the Faculty of Science  
(Professor Polkit Sangvanich, Ph.D.)

THESIS COMMITTEE

.....Chairman  
(Assistant Professor Warinthorn Chavasiri, Ph.D.)

.....Thesis Advisor  
(Professor Nongnuj Muangsin, Ph.D.)

.....Examiner  
(Chatr Panithipongwut Kowalski, Ph.D.)

.....External Examiner  
(Assistant Professor Nalena Praphairaksit, Ph.D.)

จุฬาลงกรณ์มหาวิทยาลัย  
CHULALONGKORN UNIVERSITY

ขวัญเรือน จันทรเพ็ญ : การสังเคราะห์อนุภาคระดับนาโนเมตรของเพอราริน-ทองคำสำหรับการนำส่งทางผิวหนัง (SYNTHESIS OF PUERARIN-GOLD NANOPARTICLES FOR TRANSDERMAL DELIVERY) อ.ที่ปรึกษาวิทยานิพนธ์หลัก: ศ. ดร.นงนุช เหมืองสิน, หน้า.

เพอรารินเป็นยาสมุนไพร มีคุณสมบัติในการต้านอักเสบ แต่เพอรารินละลายน้ำได้น้อยจึงทำให้ประสิทธิภาพในการรักษาลดลง ดังนั้นงานวิจัยนี้จึงสังเคราะห์อนุภาคทองคำระดับนาโนเมตรสำหรับนำส่งยาเพอราริน เพื่อเพิ่มการละลายและเพิ่มประสิทธิภาพในการนำส่งยาทางผิวหนัง ซึ่งสังเคราะห์ได้โดยดัดแปลงโครงสร้างของแคปป์-คาร์ราจีแนนด้วยควอท 188 ที่ความเข้มข้น 25 เปอร์เซ็นต์โดยปริมาตร จากนั้นนำแคปป์-คาร์ราจีแนนที่ดัดแปลงโครงสร้างแล้วใช้ปรับเสถียรและการสังเคราะห์อนุภาคทองคำระดับนาโนเมตรต่อไป สามารถยืนยันโครงสร้างแคปป์-คาร์ราจีแนนหลังการดัดแปลงแล้วด้วยเทคนิค  $^1\text{H}$  NMR พบเปอร์เซ็นต์การสังเคราะห์ควอท 188 บนโครงสร้างแคปป์-คาร์ราจีแนนเท่ากับ 21.21 เปอร์เซ็นต์ และมีค่าการละลายน้ำสูงถึง  $43.7 \pm 0.01$  เปอร์เซ็นต์เมื่อเทียบกับแคปป์-คาร์ราจีแนนก่อนดัดแปลงโครงสร้าง จากนั้นยืนยันขนาดอนุภาคทองคำระดับนาโนเมตรที่สังเคราะห์ได้ด้วยเทคนิคต่าง ๆ เหล่านี้ เช่น UV-vis, TEM, EDX และ DLS พบขนาดอนุภาคทองคำระดับนาโนเมตรเท่ากับ 15 นาโนเมตร ศึกษาฤทธิ์ทางชีวภาพของตัวยาที่ถูกไหลลดลงบนอนุภาคทองคำระดับนาโนเมตร พบว่าระบบนำส่งยาที่สังเคราะห์ขึ้นสามารถนำส่งยาเพอรารินเข้าสู่เซลล์ได้แล้วจำเพาะกับเซลล์ CLS และไม่มีความเป็นพิษต่อเซลล์ปกติ ทดสอบการซึมผ่านผิวหนังของระบบนำส่งยาที่สังเคราะห์ขึ้นด้วยวิธีฟรานซ์เซลล์และพิสูจน์เอกลักษณ์ของอนุภาคที่ซึมผ่านเมมเบรนด้วยเทคนิค ICP-OES and UV-vis พบว่าระบบนำส่งยาที่สังเคราะห์ขึ้นสามารถนำส่งเพอรารินผ่านผิวหนังได้ ดังนั้นจากผลการทดลองทั้งหมดจึงสามารถยืนยันได้ว่าสามารถสังเคราะห์ระบบนำส่งยาที่เพิ่มการละลายน้ำและเพิ่มการนำส่งยาผ่านผิวหนังได้สำเร็จ เพราะฉะนั้นจึงสามารถนำระบบนำส่งยานี้ไปประยุกต์ใช้กับการนำส่งยาต่อไปได้

สาขาวิชา ปีโตรเคมีและวิทยาศาสตร์พอลิเมอร์ ลายมือชื่อนิสิต .....

ปีการศึกษา 2560

ลายมือชื่อ อ.ที่ปรึกษาหลัก .....

# # 5771925223 : MAJOR PETROCHEMISTRY AND POLYMER SCIENCE

KEYWORDS: TRANSDERMAL DELIVERY / GOLD NANOPARTICLES / KAPPA-CARRAGEENAN / SOLUBILITY / ELECTROSTATICAL

KWANRUEN CHANPENG: SYNTHESIS OF PUERARIN-GOLD NANOPARTICLES FOR TRANSDERMAL DELIVERY. ADVISOR: PROF. NONGNUJ MUANGSIN, Ph.D., pp.

Puerarin (Pur) is herbal medicine that its inflammatory response but low solubility to reduce activity. Thus, the aim of this study was to synthesize q188-kappa-carrageenan@Pur@gold nanoparticles (q188-**K-c**@Pur@AuNPs) for enhancing solubility and transdermal delivery. The **K-c** was synthesized by quaternization of **K-c** with 25% (v/v) q188, and the q188-**K-c** @AuNPs was prepared by reducing H<sub>2</sub>AuCl<sub>4</sub> into AuNPs by using 25% (v/v) q188-**K-c** as reducing and stabilizing agents. The highest degree of quaternization (%DQ) at 21.12% was found q188 addition, which was calculated from <sup>1</sup>H NMR. The solubility of the q188-**K-c** derivatives was 43.7±0.01%, which higher than **K-c**. The size of synthesized q188-**K-c**@AuNPs was confirmed by UV-vis, TEM, EDX and DLS, which were found the successfully synthesized with the size 15 nm. A cytotoxic study of Pur loaded on q188-**K-c**@AuNPs derivatives (q188-**K-c**@Pur@AuNPs) were observed, which shown increasing cytotoxicity to CLS cells and non-toxic to normal cells (Wi-38) by MTT assay. *In vitro* drug permeation was studied by Franz's cell method. The q188-**K-c**@Pur@AuNPs permeation was investigates by ICP-OES and UV-vis that shown increasing permeation to across cellulose membrane. According to the results, it was suggested that q188-**K-c**@Pur@AuNPs can be a good candidate to further development for transdermal delivery applications.

Field of Study: Petrochemistry and  
Polymer Science

Student's Signature .....

Advisor's Signature .....

Academic Year: 2017

## ACKNOWLEDGEMENTS

The author thanks many people for kindly providing the knowledge of this study. First of all, I would like to express gratitude and appreciation to my advisor, Professor Dr. Nongnuj Muangsin for invaluable guidance and suggestions throughout this work. I wish to express my grateful thank to Assistant Professor Dr. Warinthorn Chavasiri chairman of thesis committee from the Department of Chemistry, Dr. Chatr Panithipongwut Kowalski examiner for the valuable advice from Department of Materials Science, I also express my appreciation to Assistant Professor Dr. Nalena Praphiraksit from Srinakharinwirot University, the thesis external examiner, for her valuable comments and suggestions.

I also thank to Dr. Kissana Siraleartmukul and Dr. Pranee Lertsutthiwong from the Center of Chitin-Chitosan Biomaterial, Metallurgy and Materials Science Research Institute of Chulalongkorn University for suggestion throughout this work.

In addition, I would like to sincere thanks to Mrs. Songchan Phutong at the institute of Biotechnology and Genetic Engineering (IBGE), Chulalongkorn University. I am grateful for kind supports, teaching the research methodologies about biological test and affectionate encouragement. Thanks also go to the members in research group, it has been enjoyable moment with you all. I appreciate friendship and single meaningful suggestion of all you.

Furthermore, the other also thanks the Program of Petrochemistry and Polymer Science, Department of Chemistry, Department of Microbiology, and the Center of Chitin-Chitosan Biomaterial, Metallurgy and Materials Science Research Institute Chulalongkorn University for providing the equipment, chemicals and facilities.

Finally, I would like to express my honest thanks to my family, and my friend for their help, support, endless love, understanding and encouragement. My thanks also given to all of those whose names have not been mentioned, for helping me to make this work complete.

## CONTENTS

	Page
THAI ABSTRACT .....	iv
ENGLISH ABSTRACT .....	v
ACKNOWLEDGEMENTS .....	vi
CONTENTS .....	vii
LIST OF ABBREVIATIONS .....	1
LIST OF TABLES .....	1
LIST OF FIGURES .....	1
CHAPTER I INTRODUCTION.....	3
1.1 Introduction .....	3
1.2 Scope of this research.....	6
1.3 The objectives of research.....	8
CHAPTER II THEORY AND LITERATURE REVIEWS .....	9
2.1 Inflammation .....	9
2.2 The gold nanoparticles (AuNPs).....	10
2.3 Localized Surface Plasmon Resonance (LSPR).....	11
2.4 Aggregation of gold Nanoparticles (AuNPs).....	12
2.5 kappa-carrageenan ( <b>K-c</b> ) .....	14
2.6 Transdermal delivery.....	15
2.7 The mucoadhesive interaction.....	16
2.8 Franz's cell apparatus .....	16
2.9 Swelling Controlled Release .....	17
2.10 Nitric oxide (NO) determination .....	18

	Page
2.11 MTT Assay.....	19
CHAPTER III EXPERIMENTAL.....	20
3.1 Materials and chemicals .....	20
3.1.1 Polymer.....	20
3.1.2 Model drug.....	20
3.1.3 Solvents and chemical .....	20
3.1.4 Cell culture apparatus.....	21
3.1.5 Cell line.....	21
3.1.6 Media and Enzyme for cell line.....	21
3.1.7 MTT assay materials and Apparatus .....	22
3.2 Instruments.....	22
3.3 Analytical Instrument .....	23
3.3.1 Proton nuclear magnetic resonance spectroscopy ( $^1\text{H}$ NMR).....	23
3.3.2 Fourier transformed infrared spectroscopy (FT-IR, ATR mode).....	23
3.3.3 Dynamic light scattering (DLS).....	23
3.3.4 Ultraviolet-Visible (UV-vis) spectroscopy .....	23
3.3.5 Transmission Electrons Microscope (TEM).....	24
3.3.6 Energy Dispersive X-ray Spectrometry (EDX).....	24
3.3.7 Inductively Coupled Plasma Optical Emission Spectrometry (ICP-OES) ...	24
3.3.8 Zeta-potential analysis .....	24
3.4 The experimental methods .....	25
3.4.1 The development of <b>K</b> -c and its derivatives .....	27
3.4.1.1 The synthesis of quaternization kappa-carrageenan (q188- <b>K</b> -c)....	27



	Page
3.4.1.2 The calculation of degree of quaternization (%DQ) .....	28
3.4.1.3 The confirmation of <b>K-c</b> and its derivatives.....	28
3.4.2 The synthesis and characterization of q188- <b>K-c</b> @AuNPs .....	29
3.4.2.1 Synthesis of q188- <b>K-c</b> @AuNPs .....	29
3.4.2.2 Characterization of q188- <b>K-c</b> @AuNPs as a confirmed .....	29
3.4.3 Preparation of q188- <b>K-c</b> @Pur@AuNPs derivatives and q188- <b>K-c</b> @Pur@AuNPs .....	29
3.4.3.1 The synthesis of q188- <b>K-c</b> @Pur@AuNPs .....	29
3.4.3.2 Characterization of q188- <b>K-c</b> @Pur@AuNPs as a confirmed .....	30
3.4.4 Anti-inflammatory activity .....	30
3.4.4.1 Cell culture.....	30
3.4.4.2 Calibration curve of nitrite standard.....	30
3.4.4.3 NO determination.....	30
3.4.4.4 Cytotoxicity by MTT assay .....	31
3.4.4.5 Determination of the anti-inflammatory .....	31
3.4.5 Swelling Controlled Release.....	32
3.4.6 <i>In vitro</i> study of drug permeation through cellulose membrane .....	32
CHAPTER IV RESULTS AND DISCUSSION .....	33
4.1 The synthesis of quaternization of q188- <b>K-c</b> and characterizations .....	33
4.1.1 <sup>1</sup> H NMR analysis.....	33
4.2 Swelling Controlled Release.....	36
4.2.1 The solubility of <b>K-c</b> and q188- <b>K-c</b> with PBS for pH 7.4 .....	36
4.3 Zeta-potential analysis.....	37

	Page
4.4 The synthesis of q188- <b>K</b> -c@AuNPs .....	38
4.4.1 Ultraviolet-visible (UV-vis) spectroscopy.....	38
4.4.2 FT-IR spectroscopy (ATR mode) analysis .....	41
4.4.3 Dynamic light scattering (DLS).....	42
4.4.5 Energy Dispersive X-ray Spectrometry (EDX).....	44
4.5 The synthesis of q188- <b>K</b> -c@Pur@AuNPs .....	45
4.5.1 FT-IR spectroscopy (ATR mode).....	45
4.6 Biological activities of q188- <b>K</b> -c@Pur@AuNPs with cancer and inflammatory cell .....	47
4.6.1 Cytotoxicity study of q188- <b>K</b> -c@Pur@AuNPs.....	47
4.7 <i>In vitro</i> study of synthesise of q188- <b>K</b> -c@Pur@AuNPs permeation through cellulose membrane by Franz's cell diffusion method .....	48
CHAPTER V CONCLUSION .....	54
REFERENCES .....	55
APPENDIX (A) .....	59
APPENDIX (B) .....	60
APPENDIX (D).....	61
VITA.....	62

## LIST OF ABBREVIATIONS

cm	Centimeter
cm <sup>-1</sup>	Unit of wavenumber
°C	Degree Celsius
D <sub>2</sub> O	Dideuterium oxide
DCC	N, N'-Dicyclohexylcarbodiimide
DMEM	Dulbecco's modified Eagle's medium
MTT	3-(4, 5-dimethylthiazol-2-yl)-2,5-diphenyltetrazolium bromide
DMSO	Dimethyl sulfoxide
h	hour
g	gram
LPS	lipopolysaccharide
L	liter
mg	milligram
v/v	volume/volume
ppm	milligram per liter
μL	microliter
μm	micrometer (s)
μM	micromolar
mL	milliliter
nm	nanometer
NO	Nitric oxide
NSAIDs	Non-steroidal anti-inflammatory drug
<sup>1</sup> H NMR	Proton Nuclear Magnetic Resonance
FT-IR	Fourier-Transform Infrared Spectroscopy
TEM	Transmission Electron Microscopy
DLS	Dynamic light scattering
DQ	Degree of quaternization
AuNPs	Gold nanoparticles

$\kappa$ -c	kappa-carrageenan
q188	3-chloro-2-hydroxypropyl trimethyl ammonium chloride
Pur	Puerarin
q188- $\kappa$ -c	quat188-kappa-carrageenan
q188- $\kappa$ -c@Pur@AuNPs	quat188-kappa-carrageenan@puerarin@gold nanoparticles



## LIST OF TABLES

<b>Table 1</b> Instruments list.....	22
<b>Table 2</b> The concentration of q188 were varied as q188- <b>K</b> -c derivatives .....	28
<b>Table 3</b> The solubility studied of synthesise of q188- <b>K</b> -c with difference concentration of q188 .....	36
<b>Table 4</b> The size distribution of q188- <b>K</b> -c@AuNPs derivatives and q188- <b>K</b> - .....	43
<b>Table 5</b> <i>In vitro</i> cytotoxic of compound against CLS, SW 620, Chago-K1, KATO III and RAW 26.7. ....	47
<b>Table 6</b> Flux relation of Au <sup>0</sup> in q188- <b>K</b> -c@Pur@AuNPs compare with q188- <b>K</b> -c@AuNPs.....	50
<b>Table 7</b> Flux relation of Pur in q188- <b>K</b> -c@Pur@AuNPs compare with <b>K</b> -c@Pur@AuNPs.....	52
<b>Table 8</b> %Flux relation of each compound was permeating through one area division .....	53
<b>Table 9</b> Flux relation between amounts of q188- <b>K</b> -c@Pur@AuNPs, q188- <b>K</b> -c@AuNPs and <b>K</b> -c@AuNPs permeating through one area division of cellulose membrane and times.....	59
<b>Table 10</b> Flux relation between amounts of q188- <b>K</b> -c@Pur@AuNPs, <b>K</b> -c@Pur@AuNPs and Pur permeating through one area division of cellulose membrane and times. ....	60

## LIST OF FIGURES

<b>Figure 1</b> Structure and pathways through of skin.....	4
<b>Figure 2</b> The structure of 3 types of carrageenan [4] .....	5
<b>Figure 3</b> Structure of puerarin (Pur).....	6
<b>Figure 4</b> Schematic of synthesis AuNPs: (A) q188- <b>K</b> -c derivatives, (B) The synthesized of q188- <b>K</b> -c@AuNPs, (C) The synthesized of q188- <b>K</b> -c@Pur@AuNPs.....	8
<b>Figure 5</b> Inflammation is a fundamental process for human survival. ....	10
<b>Figure 6</b> The spectra of AuNPs in different sizes.....	11
<b>Figure 7</b> Schematic were shown of a LSPS of spherical AuNPs. ....	12
<b>Figure 8</b> The accumulation of circulating gold nanoparticle conjugates at tumor sites.....	13
<b>Figure 9</b> The components of Franz’s cell [18] .....	17
<b>Figure 10</b> Schematic presentation of swelling as a preparation for controlled drug release.....	18
<b>Figure 11</b> Mitochondrial reduction of MTT to blue formazan product.....	19
<b>Figure 12</b> The schematic of methods and materials in experimental procedures are divided into III parts.....	26
<b>Figure 13</b> Schematic representation of <b>K</b> -c and q188- <b>K</b> -c derivatives.....	27
<b>Figure 14</b> Structure of Kappa-carrageenan ( <b>K</b> -c) .....	33
<b>Figure 15</b> <sup>1</sup> H NMR spectra of (a) <b>K</b> -c, (b) q188, (c-f) 10, 25, 50, 75 % (v/v) q188- <b>K</b> -c .	35
<b>Figure 16</b> Presentation of swelling controlled release[2].....	36
<b>Figure 17</b> Zeta-potential analysis of (a) <b>K</b> -c and (b) q188- <b>K</b> -c derivatives as a modified .....	37

<b>Figure 18</b> The absorption spectra of q188- <b>K-c</b> @AuNPs were measured at wavelength range of 200-700 nm on microtiter plate reader; (A) pure <b>K-c</b> , (B) solution of H <sub>2</sub> AuCl <sub>4</sub> , (C) 1% (w/v) <b>K-c</b> with H <sub>2</sub> AuCl <sub>4</sub> solution, (D) 10% (v/v) q188- <b>K-c</b> @AuNPs, (E) 25% (v/v) q188- <b>K-c</b> @AuNPs, (F) 50% (v/v) q188- <b>K-c</b> @AuNPs and (G) 75% (v/v) q188- <b>K-c</b> @AuNPs.....	39
<b>Figure 19</b> The absorption spectra of q188- <b>K-c</b> @AuNPs were measured at wavelength.....	40
<b>Figure 20</b> FT-IR spectra of (a) <b>K-c</b> , (b) q188, (c) 25% (v/v) q188- <b>K-c</b> used as various.....	41
<b>Figure 21</b> The morphology of q188- <b>K-c</b> @AuNPs a) the particle size of q188- <b>K-c</b> @AuNPs from histogram, b-d) the sphere and particle sized of q188- <b>K-c</b> @AuNPs....	43
<b>Figure 22</b> Characterization of the gold nanoparticles formed by the reaction of 25% (v/v) q188- <b>K-c</b> @AuNP: Spot profile EDX spectrum. ....	44
<b>Figure 23</b> FT-IR spectra of: (a) 25% (v/v) q188- <b>K-c</b> @AuNPs, (b) Puerarin and 25% (v/v).....	46
<b>Figure 24</b> Cumulative release of Au <sup>0</sup> from q188- <b>K-c</b> @Pur@AuNPs compare with q188-.....	49
<b>Figure 25</b> Cumulative release of Pur in q188- <b>K-c</b> @Pur@AuNPs compare with .....	51
<b>Figure 26</b> Flux relation between amounts of q188- <b>K-c</b> @Pur@AuNPs, q188- <b>K-c</b> @AuNPs.....	59
<b>Figure 27</b> Flux relation between amounts of q188- <b>K-c</b> @Pur@AuNPs, <b>K-c</b> @Pur@AuNPs.....	60
<b>Figure 28</b> Calibration Curve of Au <sup>0</sup> from Franz's cell method by ICP-OES.....	61
<b>Figure 29</b> Calibration Curve of puerarin from Franz's cell method by UV-vis.....	61

# CHAPTER I

## INTRODUCTION

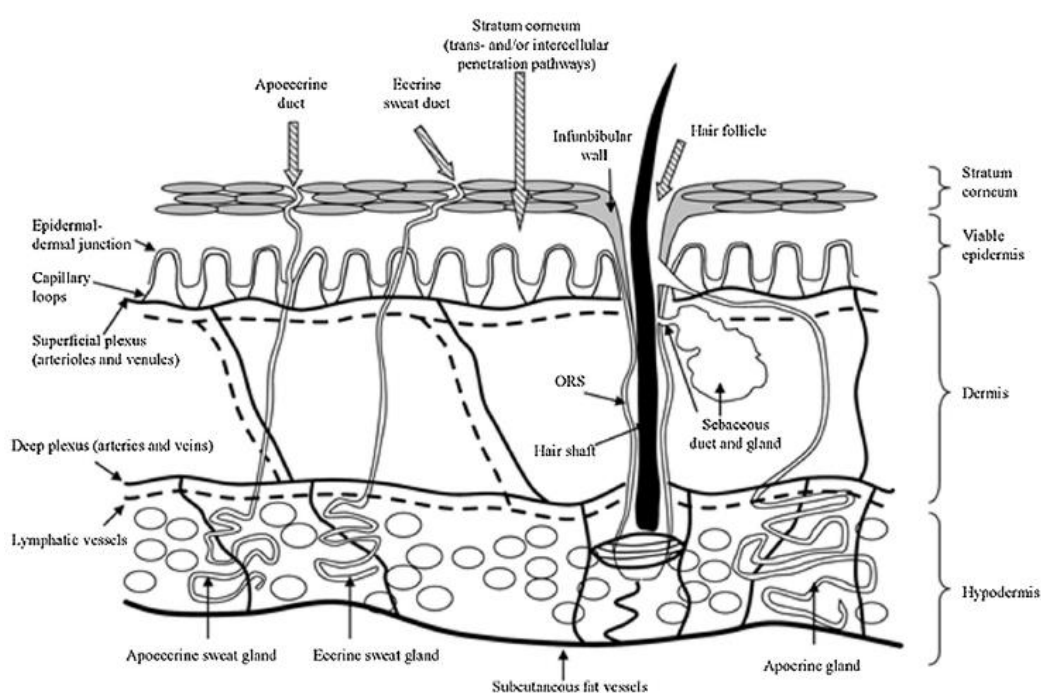
### 1.1 Introduction

Transdermal delivery has many important advantages such as protects the active compound from gastric enzymes, easy, painless and avoids the hepatic first-pass effect. The composed of skin is epidermis, dermis and hypodermis. The dermis was essential for transdermal delivery of therapeutic agents because its blood vessels and lymphatic gland composited. The pathways through of skin can be classified as intercellular routes, intracellular routes and appendage routes (Figure1).[1] However, the transdermal delivery system was showed limited of skin penetration ability because only a small of drug molecules and high solubility can be through skin. The previous research, nanoparticles technology with small size can be enhanced the permeability of drug molecules through epidermis to dermis.

The properties of gold nanoparticles (AuNPs) such as chemical, physical, optical, and electronic can be applied to various fields, which provided in pharmaceutical applications as drug delivery systems. The AuNPs can controlled of a wide range of sizes from 1 nm to 200 nm. Moreover, The AuNPs can be easily modified with controlled dispersal including as an ease of functionality target tissue specificity and non-toxic of Au (III) metal. Thus, AuNPs have a great potential to be used as a drug delivery system for efficient drug transport into different cell types. The size of AuNPs determine the optical property in UV absorbance and the red wine color. However, the step to synthesis of AuNPs via chemical and physical method involved difficult approaches to expensive and toxic from reducing agent that are not suitable for drug delivery applications. Consequently, the biopolymer was another choice for synthesis of gold nanoparticles that its non-toxic for reducing and stabilizing agents and low cost. One of biopolymer is carrageenan that its many application in the industry such as pharmaceutical, food and cosmetic industry. In the last decade, the carrageenan has been investigated as a carrier for controlled drug release. Previous studies indicate that



biopolymer used as reducing agent for synthesis of AuNPs. Therefore, we have modification positive charge on  $\kappa$ -c backbone that anionic biopolymer for synthesis AuNPs (q188- $\kappa$ -c@AuNPs). The  $\kappa$ -c and its derivatives were reducing agent and stabilizing agent without toxic reagent. The q188- $\kappa$ -c@AuNPs in order to increase electrostatic interaction with cell membrane. Hence, the synthesized of q188- $\kappa$ -c@AuNPs can be enhance permeation of Pur to transdermal delivery systems.[2]



CHULALONGKORN UNIVERSITY  
**Figure 1** Structure and pathways through of skin.

The carrageenan is a biopolymer occurring anionic sulfated linear polysaccharides extracted from marine red algae. According to the literature investigate, mainly of carrageenan can be classified in 3 types (Figure 2.) that kappa-carrageenan ( $\kappa$ -c), lambda-carrageenan ( $\lambda$ -c) and Iota-carrageenan ( $\iota$ -c) depend on the amount and position of sulfated group cause to difference properties. The  $\kappa$ -c is mainly used as supporting materials for controlled drug delivery system, food and cosmetic industry as gelling, thickening and stabilizing agent due to its biocompatibility, biodegradability

and non-toxicity [3]. Moreover, the  $\kappa$ -c was interested in transdermal delivery system because  $\kappa$ -c can permeation to skin via ionic interactions and non-toxic. Therefore, the  $\kappa$ -c can be used enhance as permeation to transdermal delivery system.

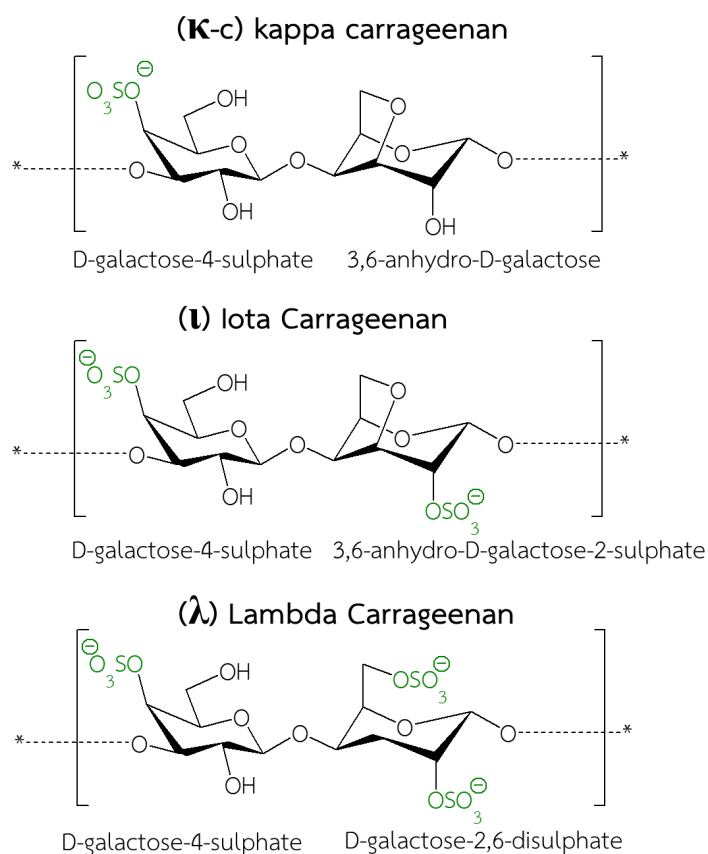


**Figure 2** The structure of 3 types of carrageenan [4]

Puerarin (Pur) (Figure 3) is herbal medicine that it can inflammatory response. Additionally, Pur has been reported to be increases insulin sensitivity and protects pancreatic islets. [6]

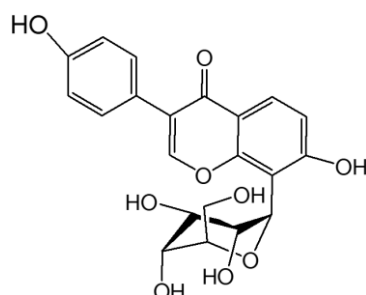


**Figure 3** Structure of puerarin (Pur)

Thus, the objective of this work is to synthesize q188- $\kappa$ -c@Pur@AuNPs for enhance transdermal delivery based on the size of gold nanoparticles and high solubility.

### 1.2 Scope of this research

The scope of this research was carried out by stepwise methodology as follows:

- The preparation of  $\kappa$ -c derivatives (q188- $\kappa$ -c) using q188 by various concentration of q188 such as 10, 25, 50 and 75 %(v/v) of q188 and characterization of q188- $\kappa$ -c by  $^1\text{H}$  NMR. Then, the synthesized of q188- $\kappa$ -c derivatives was confirmed soluble by Solubility test.
- The synthesis of gold nanoparticles used as a reducing and stabilizing of q188- $\kappa$ -c derivatives. The characterization was confirmed of q188- $\kappa$ -c@AuNPs by UV-vis, TEM, EDX, Zeta potential and DLS.
- The preparation and preliminary cytotoxic study of Pur load on q188- $\kappa$ -c@AuNPs derivatives (q188- $\kappa$ -c@Pur@AuNPs) for evaluation of biological. The study the cytotoxicity of q188- $\kappa$ -c@Pur@AuNPs with CLS (oral cancers), Chago-K1 (lung carcinoma), KATO III (stomach carcinoma), RAW 264.7 (inflammatory) and normal cell (Wi-38) by MTT assay.

- In *vitro* drug permeation of q188-κ-c@Pur@AuNPs was studied through cellulose membrane as a barrier in phosphate buffered saline pH 7.4 at  $37\pm 1^\circ\text{C}$  using by Franz's cell method. The q188-κ-c-@Pur@AuNPs permeation was investigates by ICP-OES and UV-vis.





## CHAPTER II

### THEORY AND LITERATURE REVIEWS

#### 2.1 Inflammation

Inflammation is process to response of tissues to toxic substances or injured tissue showed in Figure 5. The physical symptoms of inflammation can be observed from swelling, redness, heat, pain and loss of function of tissue. The intermediate of inflammation is responded was leukotrienes, bradykinin, interleukins and substance with oxygen molecules (Reactive Oxygen Species; ROS) produced by white blood cells (neutrophils) that important role in the destruction of pathogens. So, the physical injury and the spread of injury was protected tissue by inflammation, which two types of inflammation was acute and chronic inflammation [7].

The acute inflammation response to intermediates instantly. It will stimulate some substance to prevent occurring harmful, the expansion of the blood vessels, increasing the flow of blood in the injured tissue which related to increasing of white blood cells, increasing the expression of adhesion molecules on endothelial cells [8]. After that, the white blood cells swallow bacteria or antigen. The ROS and proteases enzyme are released. These may cause more damaged tissue [9]. The effect of these processes in the production of chemical mediators of inflammation and lead to more inflammation, too. This cytokine is response for regulation of white blood cells or inhibited the response of the immune system, which have protected inflammation. The inflammation is eliminated by white blood cells that will move to the area of injury and apoptosis.

The chronic inflammation can occur for a long time. The changing nature of the inflammatory cell types by region. Examples of diseases caused by chronic

inflammation include rheumatoid arthritis, asthma and inflammatory bowel disease and many other diseases associated with inflammation (atherosclerosis, autoimmune diseases, Alzheimer's disease, cancer, trauma, ischemia, diabetes, etc.) [10, 11], which need to be treated with antibiotics in the steroids group. However, there are side effects to the patient. Furthermore, the antibiotics in nonsteroidal anti-inflammatory drugs (NSAIDs) group is commonly used to cure the disease but there are side effects to the stomach. Pur were interested in the study of biological activities.

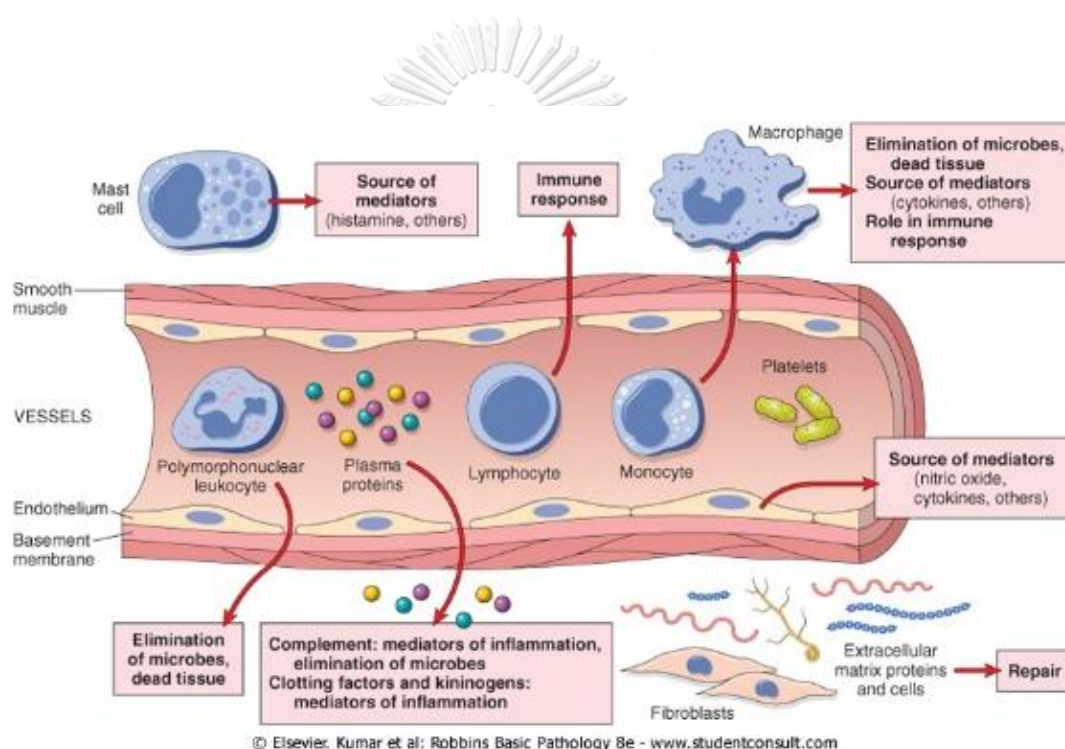


**Figure 5** Inflammation is a fundamental process for human survival.

## 2.2 The gold nanoparticles (AuNPs)

In the recent, the nanoparticles technology used as prepare drug delivery because its non-toxic carriers for drug delivery application. The sized of AuNPs used as a determination the optical property by UV absorbance (Figure 6, 7) and investigate from red-wine color of colloid solution. [12] The AuNPs were shown red-wine color because

of localized surface plasmon resonance (LSPR) band around 520 nm in the visible region.

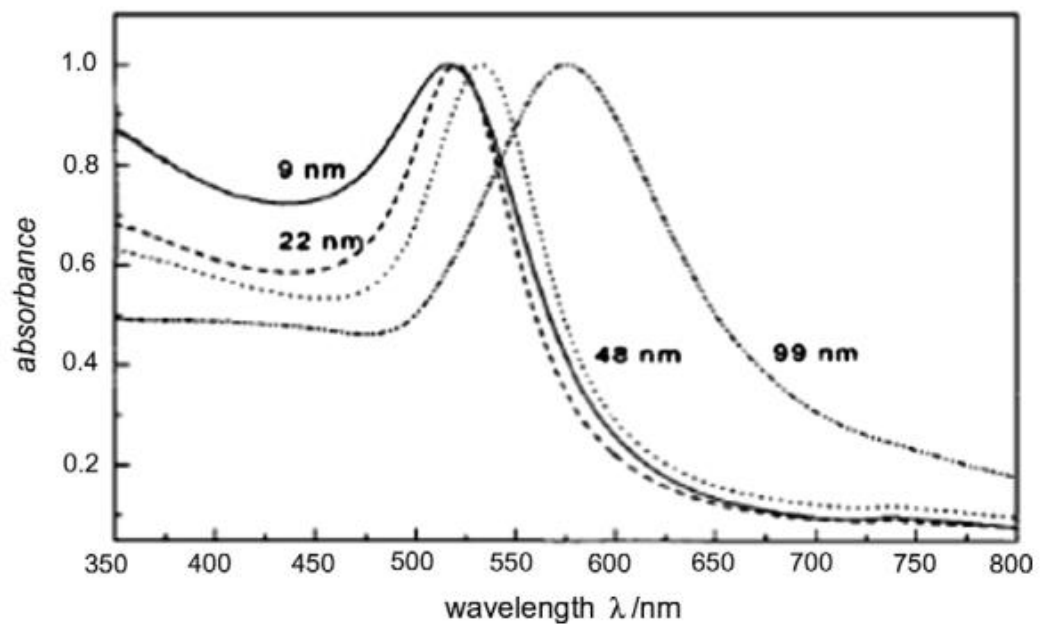


**Figure 6** The spectra of AuNPs in different sizes.

### 2.3 Localized Surface Plasmon Resonance (LSPR)

LSPR is an optical property for nanoparticles which demonstrated of the interaction of the electron cloud in AuNPs with electric field of light of resonant frequency. The Figure 7 were shown interaction of light wave which alternating electric field and affective electrons in AuNPs. As a result of the absorption of resonant light are free electrons of gold exhibit a collective coherent oscillation around the nanoparticle surface. This coherent oscillation induced as a result of the absorption of light in resonance with the incident light. Spherical of AuNPs with 5 to 80 nm size have extinction band around 520 nm in the visible region and give red-wine color.



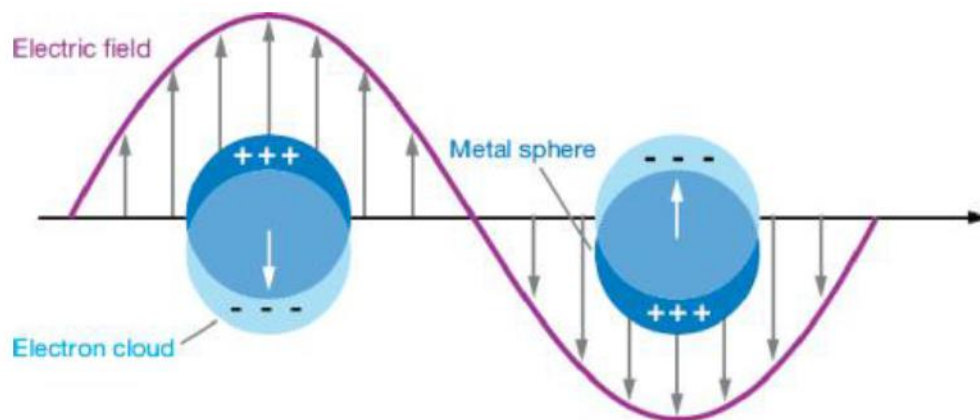


**Figure 7** Schematic were shown of a LSPS of spherical AuNPs.

#### 2.4 Aggregation of gold Nanoparticles (AuNPs)

The theories of colloidal stability can be explaining aggregation be heavier of AuNPs. The colloid stability theory, the AuNPs can be combine with itself by effect of van der Waals attraction and electrostatic repulsion. The theory of colloid stability is to mention them in the term of interaction energy as showed in equation (1)

The aggregation behavior of AuNPs can be explained by theories of colloidal stability. The colloid stability can be provided by DLVO theory. In this theory, the aggregation of AuNPs have include the effect of van der Waals attraction and electrostatic repulsion. The easier representation of this theory is to mention them in the term of interaction energy.

$$E_t = [E_a + E_r] \quad (1)$$

where  $E_t$  is the total interaction energy that it should be the positive value if the total energy in negative value will be aggregate of particles.  $E_a$  is the van der Waals attraction energy that its negative value.  $E_r$  is the electrostatic repulsion potential energy.

The size of AuNPs is also an important parameter for drug delivery and conjugates in blood circulation. Previous studies indicate that 10 nm of AuNPs can circulate in blood more than 24 hours in animals, but other sizes of AuNPs remain for a shorter time. In addition to stability in blood, the size of AuNPs is also strongly associated with cytotoxicity and aggregation in blood cells (Figure 8). According to Jungshan Chang have studied triphenylphosphine coated AuNPs at a size of 1.4 nm display the most cytotoxicity by inducing cell necrosis on tissue fibroblasts, epithelial cells, macrophages, and melanoma cells as compared to larger AuNPs. Moreover, the tissue specificity and the biodistribution of AuNPs are decided by the cell surface properties, underlining the ratio of endocytosis and exocytotic activity among cells. However, the relatively larger sizes of AuNPs at diameters of 50 nm or 200 nm exhibit non-toxicity with animals.

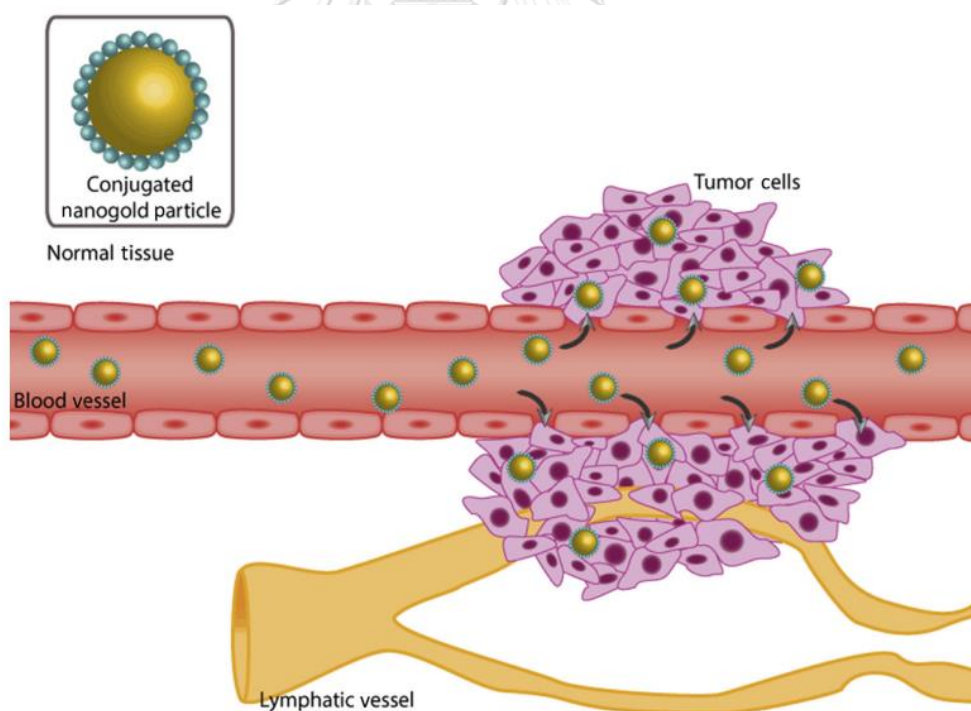


**Figure 8** The accumulation of circulating gold nanoparticle conjugates at tumor sites by the enhanced permeability and retention effect.

The studies found that effect of size AuNPs as used to drug delivery systems follow:

In 2002, Hickey *et al.* [13] studied antibiotics, dexamethasone with AuNPs can reduce tissue inflammation from organ medical implantation.

In 2011, Franca *et al.* [14] reported that the AuNPs were low toxicity (0.005 EU/ml) and found that the particles do not cause the release of cytokines in white blood cells as well.

In 2013, Chen *et al.* [15] the size of AuNPs with 21 nm can be inhibit the expression of TNF- $\alpha$  in fat tissue of mice after intraperitoneal injection. It is shown that AuNPs has the anti-inflammatory activity.

In 2013, Sumbayev *et al.* [16] explained AuNPs was directly connected with IL- $1\beta$  inhibitors that its inflammation.

2.5 kappa-carrageenan ( $\kappa$ -c)

The kappa-carrageenan ( $\kappa$ -c) is one of the most abundant natural occurring polysaccharide extracted from marine red algae. It is mainly used in the food and cosmetic industry as gelling, thickening and stabilizing agent due to its biocompatibility, biodegradability and non-toxicity. The use of  $\kappa$ -c as supporting materials for controlled drug delivery system has also received considerable attention. Moreover, the  $\kappa$ -c was good materials, its shown that  $\kappa$ -c can permeation to skin via ionic interactions and non-toxic. Therefore, the  $\kappa$ -c can be used to transdermal delivery system.

The  $\kappa$ -c is not electrostatically attracted to the anionic surfaces of skin and low solubility because of their inherent anionic charge. In contrast, the functionalization of  $\kappa$ -c with cationic charge can improve its binding to keratinized surfaces of skin and enhance solubility.[17] In previously reports, the cationic groups linked to starch and cellulose derivatives were employed in industries concerned with medical products and cosmetics.

The cationic modification of polysaccharides by the cationization with 2,3-epoxypropyl trimethylammonium chloride (EPTC), which can be obtained but an unstable and toxic reagent. However, the use of low toxic reagent such as 3-chloro-2-hydroxypropyl trimethylammonium chloride (q188) was introduced. The q188 was successfully quaternized on backbone of  $\kappa$ -c. In recently, the modified of  $\kappa$ -c with cationic charge from q188 can improve its binding to keratinized surfaces of skin.

## 2.6 Transdermal delivery

The skin is an important barrier to controlled drug delivery. Transdermal delivery system is the results of sophisticated procedures, which technology prevailed over a well-known pharmacological component, resulting in the development of the system in a short time. Such development progressed through three stages, or generations, aimed at improving delivery and absorption, reducing patch size and making it easier to use. Furthermore, the therapeutic benefits of transdermal drug delivery systems are an important issue in the development of any drug products.

The advantages of transdermal delivery are:

- Adaptability to drugs with a short half-life.
- Avoidance of variation in gastrointestinal absorption.
- By pass of the hepatic first pass metabolism.
- Good patient compliance.
- Production of sustained and constant plasma concentrations of drugs
- Reduction in repeated dosing intervals.
- Reduction of potential adverse side effects.
- Removal of transdermal drug delivery systems provokes an immediate decrease of drug plasma levels.
- Substitute for oral or parenteral administration in certain clinical situation.

- Suitable for drugs which produce a therapeutic response at very low plasma concentrations.

## 2.7 The mucoadhesive interaction.

Mucus is a complex viscous adherent secretion which is synthesized by specialized goblet cells. There is composed of water and mucins which are glycoprotein of exceptionally high molecular weight. Moreover, pendant sialic acid and sulfate groups located on the glycoprotein molecules result in mucin behaving as an anionic polyelectrolyte at neutral pH. For adhesion to occur, molecule must bond across the interface. These bonds can arise by ionic interactions, van der Waals forces, covalent bonds, hydrogen bonds, and hydrophobic interactions.

Mucoadhesion is a complex process and numerous theories have been presented to explain the mechanisms involved. These theories include mechanical-interlocking, electrostatic, diffusion-interpenetration, adsorption and fracture processes.

## 2.8 Franz's cell apparatus

Franz's cell (Figure. 9) are used for *in vitro* study to quantify the release rate of drugs from topical preparation. In these systems, skin membranes or synthetic membranes may be used as barriers to the flow of drug and vehicle to simulate the biological system. The typical of Franz's cell has two chambers, one on each side of the test diffusion membrane. A temperature-controlled solution is placed in one chamber and a receptor solution in the others. Drug permeation may be determined by periodic sampling and assay of the drug content in the receptor solution. The Franz's cell is the most widely used apparatus to determine the drug release profile from the topical drug products because of the reliability and reproducibility. The test sample is placed in the donor phase, which was separated from the receptor phase by a semipermeable membrane. The suitable receptor medium is suggested to

increase the drug solubility for detection of drug release by the UV-visible spectroscopy or high-pressure liquid chromatography (HPLC)

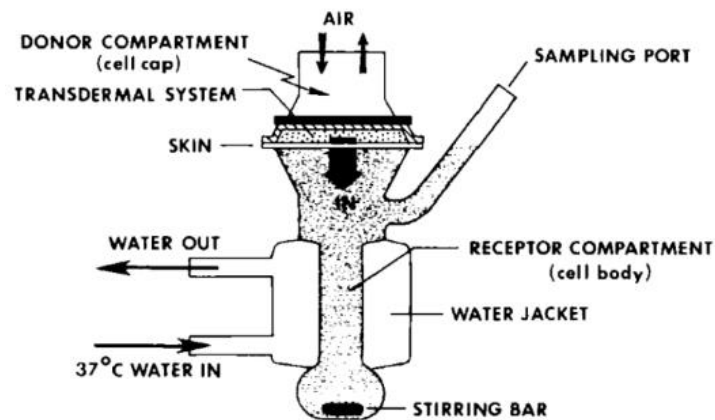
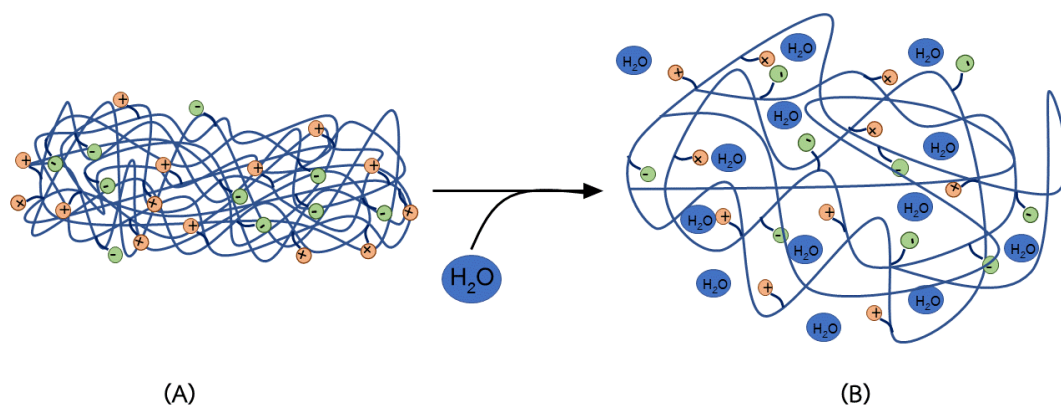


Figure 9 The components of Franz's cell [18]

## 2.9 Swelling Controlled Release

The swelling of the carrier increases the aqueous solvent content within the polymer matrix, enabling the drug to diffuse through the swollen network into the external environment. Most of materials used are based on hydrogel. The swelling can be triggered by a change in the environment surrounding such as pH, temperature and ionic strength (figure. 10)



**Figure 10** Schematic presentation of swelling as a preparation for controlled drug release.

$$\text{Swelling ratio} = \left[ \frac{W_s - W_d}{W_d} \right] \quad (2)$$

$$\text{sol fraction} = \left[ \frac{W_i - W_d}{W_i} \right] \quad (3)$$

Here,  $W_i$ ,  $W_s$ , and  $W_d$  represent the weight of dried hydrogel composites after cross linking, the weight of hydrogel composites after swelling in PBS, and the weight of dried hydrogel composites after swelling, respectively. The swelling ratio is defined as the fractional increase in the weight of the hydrogel due to water absorption. The sol fraction represents the fraction of the polymer following a crosslinking reaction that is not part of a cross-linked network. A decrease in sol fraction over time reflects polymer loss and characterizes the extent of hydrogel degradation.

#### 2.10 Nitric oxide (NO) determination

Nitric oxide (NO) is a free radical species that is intricately involved with the innate immune response [19]. NO is synthesized by nitric oxide synthase (NOS) from L-arginine using NADPH and molecular oxygen in various animal cells and tissues., is a free radical and an intercellular messenger produced by a variety of mammalian cells. NO shows cytotoxicity and tissue damage, whereas nanomolar concentrations of NO

produced by constitutive forms of NOS are essential to maintain normal cellular functions. NO is involved in various biological processes including inflammation and immunoregulation. Therefore, inhibition of NO production by iNOS may have potential therapeutic value when related to inflammation and septic shock [20].

### 2.11 MTT Assay

MTT assay is a colorimetric assay for evaluating cell metabolic activity. NAD(P)H-dependent cellular oxidoreductase enzymes may indicate the number of viable cells. These enzymes are able of reducing the yellow [3-(4,5-dimethylthiazol-2-yl)-2,5-diphenyltetrazolium bromide, MTT tetrazole dye to its insoluble [(E,Z)-5-(4,5-dimethylthiazol-2-yl)-1,3-diphenylformazan, formazan], which has a purple color in living cells. A solubilization solution (usually dimethyl sulfoxide, DMSO) is added to dissolve the insoluble purple formazan production into a colored solution. The mechanism of MTT to blue formazan product were shown Figure 11.

The absorbance of this colored solution can be quantified by measuring at a certain wavelength (usually 540 nm) by a spectrophotometer. The degree of light absorption depends on the solvent.

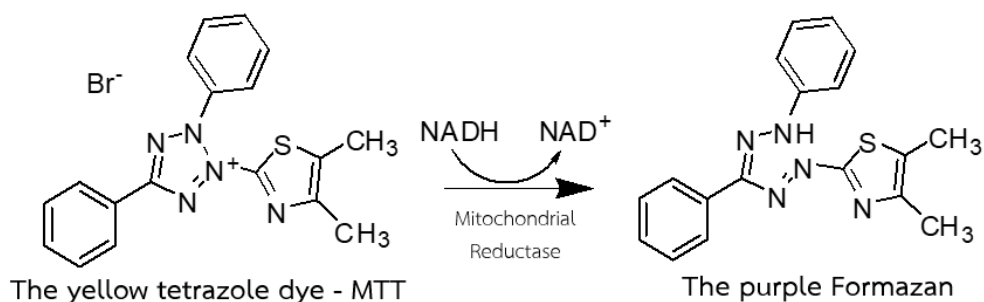


**Figure 11** Mitochondrial reduction of MTT to blue formazan product.



## CHAPTER III

### EXPERIMENTAL

#### 3.1 Materials and chemicals

##### 3.1.1 Polymer

- kappa-carrageenan ( $\kappa$ -c), food grade, 500 – 1,000 kDa, Deacetylation 95 %, Lot No.405301, (Union Chemical 1986, Thailand)

##### 3.1.2 Model drug

- Puerarin (Pur) was used in this study purchased from Xi'an Natural Field Bio-Technique Co., Ltd., China

##### 3.1.3 Solvents and chemical

- Acetone, AR grade: Merck, Germany
- 3-chloro-2-hydroxypropyl trimethyl ammonium chloride, AR grade: Merck, Germany.
- Deuterium oxide ( $D_2O$ ) for NMR, 99.9 atom % D: Merck, Germany.
- Dimethyl sulfoxide (DMSO), AR grade: Merck, Germany.
- 3-chloro-2-hydroxypropyl trimethyl ammonium chloride (q188), AR grade: TCI Chemicals, Tokyo.
- di-Sodium hydrogen phosphate ( $Na_2HPO_4$ ), AR grade: Merck, Germany.
- Ethanol absolute (EtOH), AR grade: Merck, Germany.
- Gold pellet 99.99%: Thailand's Gold Trader Association
- Hydrochloric acid fuming 37% (HCl), AR grade: Merck, Germany.
- Hydrogen tetrachloroaurate 10,000 ppm ( $HAuCl_4$ ): Homemade form gold 99.99%
- Nitric acid 65% ( $HNO_3$ ), AR grade: Merck, Germany.

- Potassium chloride (KCl), AR grade: Merck, Germany.
- Potassium dihydrogen phosphate ( $\text{KH}_2\text{PO}_4$ ), AR grade: Merck, Germany.

#### 3.1.4 Cell culture apparatus

- 96-well plates: Corning Incorporated, USA
- Centrifuge: Thermo Fisher Scientific Inc., USA
- Counting slide: Boeco, Germany
- Dropper: Isolab, Germany
- Forceps: Thermo Fisher Scientific Inc., USA
- Incubator: Thermo Fisher Scientific Inc., USA
- Lamina air flow hood: Cambridge, USA
- Microscope: Nikon, Japan
- Micropipette: Thermo Fisher Scientific Inc., USA
- Multichannel pipette: Thermo Fisher Scientific Inc., USA
- Rubber bulb: Isolab, Germany
- Vortex: Schott, Germany
- Tube: Eppendorf, Malaysia

#### 3.1.5 Cell line

- Murine Macrophage Leukemia cancer cell (RAW 264.7): Cells line Service, Germany

#### 3.1.6 Media and Enzyme for cell line

- Dulbecco's modified medium (DMEM): Sigma-Aldrich Chemistry Inc., USA
- Fetal Calf Serum (FCS): Sigma-Aldrich Chemistry Inc., USA
- Griess reagent (modified): Sigma-Aldrich Chemistry, USA
- Lipopolysaccharide (LPS): Sigma-Aldrich Chemistry, USA
- Trypsin: Thermo Fisher Scientific Inc., USA

### 3.1.7 MTT assay materials and Apparatus

- 3-(4,5-dimethylthiazol-2-yl)-2,5-diphenyltetrazolium bromide (MTT): Thermo Fisher Scientific Inc., USA
- Microplate reader spectrophotometer: Thermo Fisher Scientific Inc., USA
- Normal saline solution (NSS): Sigma-Aldrich Chemistry, USA

### 3.2 Instruments

**Table 1** Instruments list

Instruments	Manufacture
Autopipette	Fisher Scientific Inc., USA
Beaker	Isolab, Germany
Dialysis bag	Membrane Filtration Products, USA
Fourier-transform Infrared Spectroscopy (FT-IR)	Thermo, Finland
Hot air oven	Memmert, Germany
Hot plate	Becthai Bangkok Equipment & Chemical, Thailand
Magnetic stirrer:	Brand, Germany
Laboratory fume hood	Asian chemicals & engineering, Thailand
nuclear Magnetic Resonance (NMR)	Bruker, Belgium
NMR tube	Schott duran, Denmark
Pipette	Witeg, Germany
Thermometer:	Brannan, England
Vortex	Schott, Germany
ICP-OES	Thermo Scientific, iCAP 6500 ICP-OES

### 3.3 Analytical Instrument

#### 3.3.1 Proton nuclear magnetic resonance spectroscopy ( $^1\text{H}$ NMR)

The  $^1\text{H}$ -NMR spectra were measured on a Varian Mercury plus spectrometer at 400 MHz. All chemical shifts ( $\delta$ ) were reported in part per million (ppm) relative to the residual proton in solvents. Coupling constants ( $J$ ) were reported in Hertz (Hz). The  $^1\text{H}$ -NMR data were processed with the MestReNova software.

#### 3.3.2 Fourier transformed infrared spectroscopy (FT-IR, ATR mode)

FT-IR spectra were recorded on Nicolet 6700 FT-IR spectrophotometer in the region from 400 to 4000  $\text{cm}^{-1}$  at a resolution of 4  $\text{cm}^{-1}$  (32 averaged scans). FT-IR is a method of measuring infrared absorption and emission spectra. The spectral features are reported in units of wavenumber ( $\text{cm}^{-1}$ ). FT-IR information was assessed with the OMNIC software.

#### 3.3.3 Dynamic light scattering (DLS)

The particle size and the size distribution of AuNPs suspension were recorded by using a dynamic light scattering (DLS) particle size analyzer. The particle size analysis was performed after synthesis for 1 h.

#### 3.3.4 Ultraviolet-Visible (UV-vis) spectroscopy

The UV-vis spectra were recorded by using an Agilent 8453E UV-vis spectrophotometer (Agilent Technologies). The absorbance spectra were recorded in triplication. The wavelength was recorded in the range of 200–800 nm. The instrument was equipped with a quartz cell with a pathlength of 1 cm.

### 3.3.5 Transmission Electrons Microscope (TEM)

The TEM images were obtained on a transmission electron microscope (JEM-2100) operated at 120 kV and equipped with an energy dispersive X-Ray spectroscopy. TEM samples were prepared by dropping an aqueous solution onto copper grids.

### 3.3.6 Energy Dispersive X-ray Spectrometry (EDX)

The analytical technique used for the elemental analysis or chemical characterization of a sample. Scanning was performed under high vacuum and a voltage of 20 kV.

### 3.3.7 Inductively Coupled Plasma Optical Emission Spectrometry (ICP-OES)

The mass fractions of gold element were analyzed using inductively coupled plasma optical emission spectrometry (ICP-OES, iCAP 6500 ICP-OES, Thermo Scientific) and were calculated the gold concentration by using calibration curve of gold element.

### 3.3.8 Zeta-potential analysis

The surface charge of  $\kappa$ -c, q188- $\kappa$ -c derivatives was determined by zeta-potential on a Malvern zeta-potential analyzer (Malvern instrument Ltd, Zetasizer version 7.01).

### 3.4 The experimental methods

The experimental methods are divided into 3 parts as follow:

**Part I:** Modified and characterization of  $\kappa$ -c with q188 which various concentration of q188.

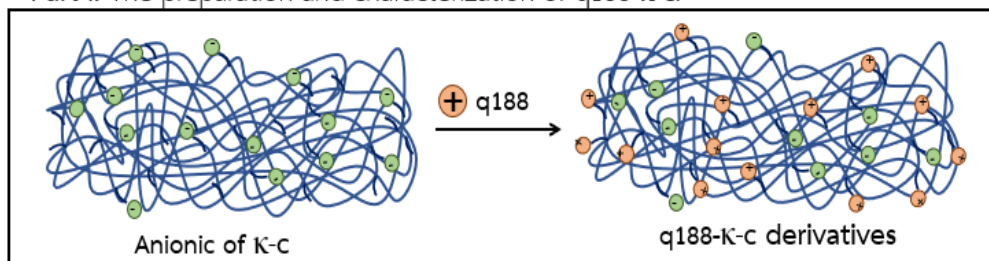
**Part II:** The preparation and characterization of q188- $\kappa$ -c and its derivatives used as reducing and stabilizer agent for synthesis of AuNPs.

**Part III:** The Preparation and preliminary were cytotoxic studied of Pur load on q188- $\kappa$ -c@AuNPs derivatives for evaluation of biological activity.

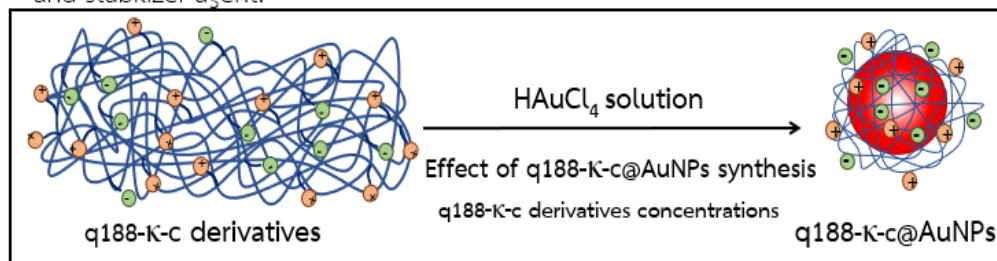
The experimental methods section is divided into 3 parts as shown in Figure 12.



**Part I:** The preparation and characterization of q188-κ-c.



**Part II:** The synthesis of q188-κ-c @AuNPs used q188-κ-c derivatives as a reducing and stabilizer agent.



**Part III:** Biological studies.

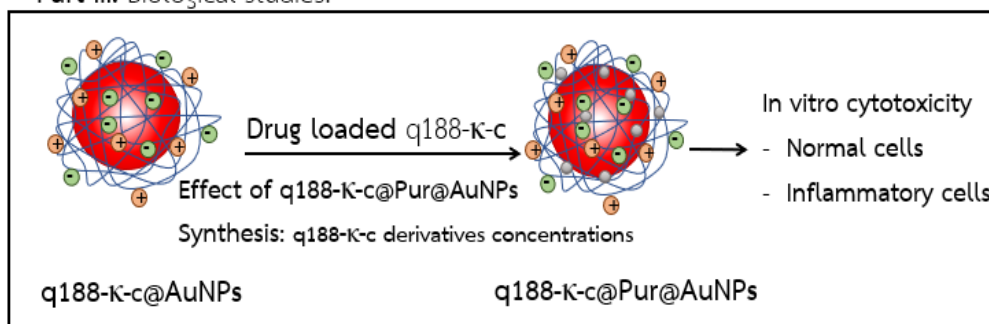


**Figure 12** The schematic of methods and materials in experimental procedures are divided into III parts.

## Part I: Modified and characterization of $\kappa$ -c with q188 which various concentration of q188.

### 3.4.1 The development of $\kappa$ -c and its derivatives

Take the first step, the anionic  $\kappa$ -c was corrected to provide positive charge from the q188 of the  $\kappa$ -c increases (Figure 13). The positive charge of  $\kappa$ -c derivatives (q188- $\kappa$ -c) used as stabilizer and enhancer permeation to cell membrane because its derivatives can be increases electrostatic interactions with negative charged of cell membranes.

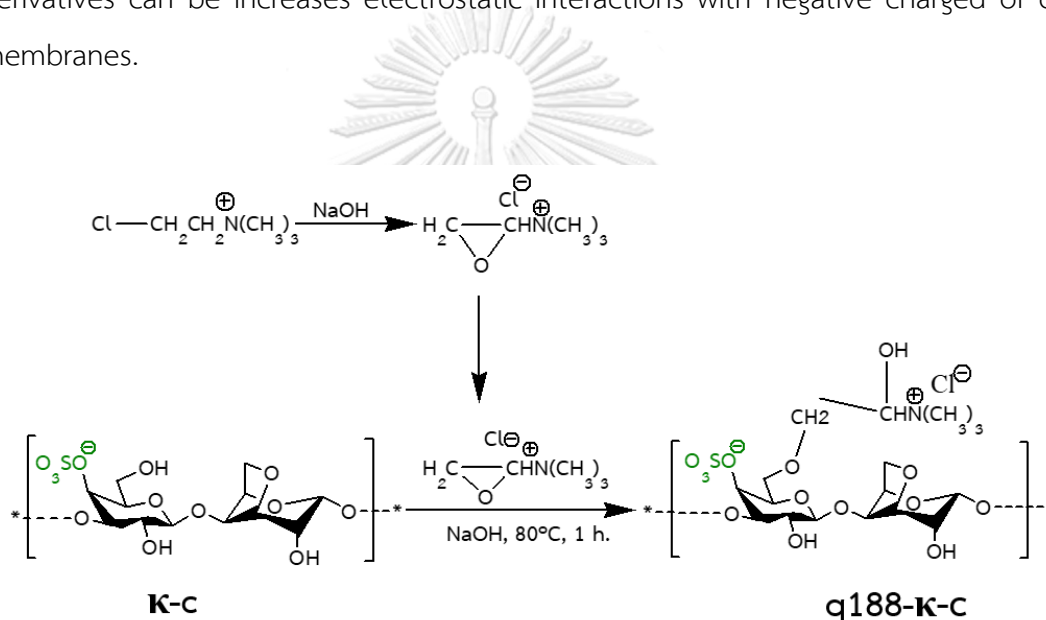


Figure 13 Schematic representation of  $\kappa$ -c and q188- $\kappa$ -c derivatives.

#### 3.4.1.1 The synthesis of quaternization kappa-carrageenan (q188- $\kappa$ -c)

The initial synthesis of q188- $\kappa$ -c, 1 g powdered  $\kappa$ -c was dissolved in 1000 mL deionized water and stirred at 70°C to observe the clear solution. Next step, 0.1 mM NaOH and q188 solution were added and continued the reaction at 70°C. The concentration of  $\kappa$ -c, q188, temperature and reaction time were varied as Table 2. The proposed mechanism of quaternization q188- $\kappa$ -c was shown in Figure 13. The product was recovered through precipitations and washed with ethanol-water (80:20) at three time. After that, the precipitate of q188- $\kappa$ -c was dialyzed (molecular weight cutoff of 6000–8000 Da) against distilled water at room temperature for one week and oven-



dried at 40°C overnight. Their product was q188-κ-c derivatives and characterized by <sup>1</sup>H NMR and FT-IR analysis.

**Table 2** The concentration of q188 were varied as q188-κ-c derivatives

κ-c (%w/v)	q188 (%v/v)
0.1	10
0.5	25
1	50
3	75

#### 3.4.1.2 The calculation of degree of quaternization (%DQ)

Their product was q188-κ-c derivatives to characterized by <sup>1</sup>H NMR. <sup>1</sup>H NMR spectra of κ-c, q188 and q188-κ-c in D<sub>2</sub>O were recorded on a Varian Mercury plus spectrometer (400 MHz). The %DQ of q188 on κ-c backbone were evaluated comparing the ratio of integral peak using as equation (4)

$$\%DQ = \left[ \frac{I(\text{He-Hg})}{I(\text{H1-H7})} \times \frac{7}{9} \right] \quad (4)$$

Where, *I* (H) and %DQ were intrigation of proton and degree of quaternization of κ-c derivatives, respectively.

#### 3.4.1.3 The confirmation of κ-c and its derivatives

The FT-IR were on record on FT-IR Nicolet 6700 in the region from 400 to 4000 cm<sup>-1</sup> wavenumber range at a resolution of 4 cm<sup>-1</sup> (32 averaged scans).

## **Part II: The preparation and characterization of q188-κ-c and its derivatives used as reducing and stabilizer agent for synthesis of AuNPs.**

### 3.4.2 The synthesis and characterization of q188-κ-c@AuNPs

#### 3.4.2.1 Synthesis of q188-κ-c@AuNPs

In a typical experiment, q188-κ-c @AuNPs was prepared by reducing  $\text{HAuCl}_4$  in the presence of 10-75% (v/v) q188-κ-c in an aqueous solution. Briefly, the synthesized of q188-κ-c 1 mL was added with 1mM  $\text{HAuCl}_4$  solution under vigorous magnetic stirring for 1h. at 70°C. The color change was occurred from colorless to wine-red colored suspension that confirmed the formation of q188-κ-c @AuNPs. The resulting wine-red solution was stored at 4 °C before use.

#### 3.4.2.2 Characterization of q188-κ-c@AuNPs as a confirmed

The absorbance was measured at wavelength range of 400-700 nm on UV-visible spectrophotometer

## **Part III: The Preparation and preliminary were cytotoxic studied of Pur load on q188-κ-c@AuNPs derivatives for evaluation of biological activity.**

### 3.4.3 Preparation of q188-κ-c@Pur@AuNPs derivatives and q188-κ-c@Pur@AuNPs derivatives as an evaluation of biological activity.

#### 3.4.3.1 The synthesis of q188-κ-c@Pur@AuNPs

The initial synthesis of q188-κ-c@Pur@AuNPs was carried out in a mixture containing at 200 ppm of Pur with q188-κ-c@AuNPs, 0.1 mL of 0.1 M NaOH and the volume was made up to 5 mL by adding the appropriate amount of deionized water. The tube was placed at magnetic stirrer and stirred to ensure the completed mixing at

80°C for 15 min. After that, solution was centrifuge precipitate were of obtain. The suspension was analyst using UV-vis spectrophotometer.

#### 3.4.3.2 Characterization of q188-κ-c@Pur@AuNPs as a confirmed

<sup>1</sup>H NMR spectra with compared of synthesized q188-κ-c and q188-κ-c@AuNPs were record in D<sub>2</sub>O on a 400 MHz NMR spectrometer.

UV-vis spectrum of q188-κ-c@Pur@AuNPs were record were recorded in triplicate. The working range was 200–800 nm.

#### 3.4.4 Anti-inflammatory activity

##### 3.4.4.1 Cell culture

The murine macrophages RAW 264.7 cells were grown in DMEM medium supplemented with 10% (v/v) of fetal bovine serum (FBS). Cultured cell lines were incubated in humidified atmosphere of 5% CO<sub>2</sub> at 37°C and then it was sub-cultured by trypsin enzyme every three days (72 h).

##### 3.4.4.2 Calibration curve of nitrite standard

The stock solution of 0.69 mg/mL sodium nitrite (NaNO<sub>2</sub>) dissolved in deionized water (DI). Then, the concentrations of nitrite performed 10 serial dilutions (0, 0.5, 1, 2, 5, 10, 20, 40, 60 and 80 μM) in triplicate down the 96-well plate (100 μL/well). Added 100 μL of Griess reagent and incubated at room temperature for 15 min (dark condition). Absorbance was measured at 540 nm on ELISA reader.

##### 3.4.4.3 NO determination

Briefly, the RAW 264.7 cells were incubated in 96-well plates at a density of  $1.44 \times 10^5$  cells/well ( $8 \times 10^5$  cells/mL) at 180 μL of Dulbecco's modified Eagle's medium (DMEM) for 24 h. After pre-incubation of RAW 264.7 cells, the DMEM medium was removed 10 μL and replaced with fresh medium containing various concentrations of compound (0-100 μM) and then were incubated with 2 μg/mL of LPS for stimulated

NO production for 24 h. The 100  $\mu\text{L}$  of supernatant was added in new 96-wells plates and mixed with 100  $\mu\text{L}$  of Griess reagent in plates. Subsequently, the mixture was incubated at room temperature for 15 min at the dark condition. The absorbance was measured at 540 nm on ELISA reader. Fresh culture medium was used as a blank in every experiment. The NO inhibitory activity can be calculated the concentration of nitrite by comparison to calibration curve of sodium nitrite standard [21].

#### 3.4.4.4 Cytotoxicity by MTT assay

The MTT colorimetric method was measured according to the procedure modified by Yang *et al.* [21]. Briefly, the murine macrophages RAW 264.7 cells were incubated in 96-well plates at a density of  $5 \times 10^3$  cells/well for 24 h. Thus, 20  $\mu\text{L}$  of treated medium was removed and added with various concentrations of treat compounds (0-100  $\mu\text{M}$ ) for 2 days. After that, the medium was incubated with 10  $\mu\text{L}$  of MTT (5 mg/mL) for 4 h. at 37°C. Hence, the supernatants were removed, the dark violet crystals were dissolved in 150  $\mu\text{L}$  of DMSO and absorbance was measured at 540 nm on ELISA reader. The percentage of dead cells was determined relative to the control group. The data that were collected for triplicates and calculated as following equation (5, 6);

$$\% \text{ Cell viability} = \frac{\text{Absorbance of treated cell}}{\text{Absorbance of untreated cell}} \times 100 \quad (5)$$

$$\% \text{ Cytotoxicity} = 100 - \text{percentage of cell viability} \quad (6)$$

#### 3.4.4.5 Determination of the anti-inflammatory

The value of absorbance ( $\text{OD}_{540}$ ) was obtained for calculation. The medical effect, or

$$\text{Inhibition rate} = 1 - \frac{\text{Absorbance of treated cell}}{\text{Absorbance of untreated cell}} \quad (7)$$

### 3.4.5 Swelling Controlled Release

The solubility of  $\kappa$ -c and q188- $\kappa$ -c in phosphate buffer (PBS) solution pH 7.4 at room temperature was calculated. For synthesized of  $\kappa$ -c and q188- $\kappa$ -c samples, 100 mg of samples were suspended in 10 mL PBS pH 7.4 and stirred at 25°C for 24 h. The undissolved solids were collected by gravity filtration, which washed in acetone and dried at 40°C under vacuum overnight. The solubility of  $\kappa$ -c and q188- $\kappa$ -c was calculated by using the following Equation (2,3).[22]

### 3.4.6 In vitro study of drug permeation through cellulose membrane

The release of q188- $\kappa$ -c@Pur@AuNPs permeation study was performed using Franz diffusion cell. Cellulose membrane with pore size of 0.45  $\mu$ m was fitted into place between the donor and receptor chambers. The upper donor chamber was filled with 12 mL of Pur loaded q188- $\kappa$ -c@AuNPs derivatives. The diameter of the Franz's cell was 1.5 cm corresponding to an effectively permeable area of 1.77 cm<sup>2</sup>. The receptor chambers contained 12 mL of acetate buffer pH 7.4 as the receptor fluid. The receptor phase was stirred at 500 rpm during the study and the temperature was maintained at 37  $\pm$  1 °C by circulating water through a jacket surrounding the cell body throughout the experiment. 500 microliter of receptor fluid was withdrawn at 0.5, 1, 2, 3, 4, 5 and 6 h. Fresh buffer was replaced after each collection. The release of Pur was analyzed using UV- visible spectroscopy at 250 nm and calculated the Pur concentration with reference calibration curve. To study release of AuNPs can be analyzed using ICP-OES and calculated the AuNPs concentration with reference calibration curve. Each test was carried out in triplicate and the mean of three observations was reported.

## CHAPTER IV

### RESULTS AND DISCUSSION

**Part I:** Modified and characterization of  $\kappa$ -c with q188 which various concentration of q188.

4.1 The synthesis of quaternization of q188- $\kappa$ -c and characterizations

4.1.1  $^1\text{H}$  NMR analysis

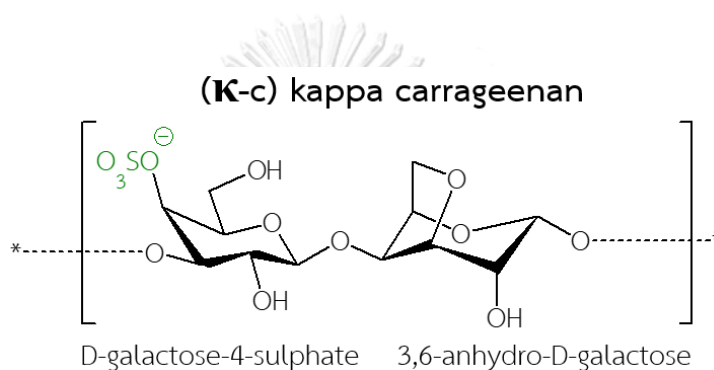


**Figure 14** Structure of Kappa-carrageenan ( $\kappa$ -c)

The structure of  $\kappa$ -c was shown in Figure. 14, which  $^1\text{H}$  NMR spectrum of  $\kappa$ -c shown in Figure.15a. The spectra of q188, 10, 25, 50 and 75% (v/v) q188- $\kappa$ -c were shown in Figure.15b, 15c, 15d,15f, respectively. The samples were dissolve in  $\text{D}_2\text{O}$ , which appeared at 4.75 ppm.

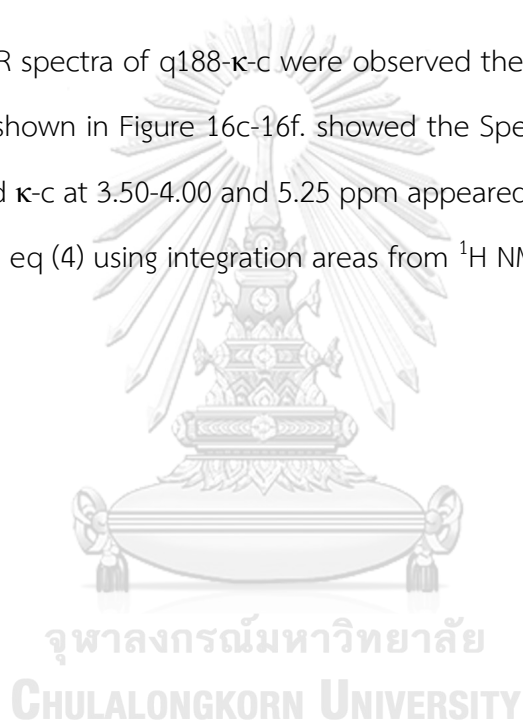
The  $^1\text{H}$  NMR spectrum of  $\kappa$ -c (Figure. 15a) showed the H1-H6 and H7 protons in D-galactose-4-sulphate at 3.50-4.00 and 5.25 ppm, respectively. The  $^1\text{H}$  NMR spectrum of q188 was shown in Figure 15b, which revealed that Hd protons in alcohol (R-OH) and Ha-Hc protons in methylene ( $-\text{CH}_2-$ ) at 4.45 and 3.50-3.75 ppm, respectively. Moreover, Specific protons of He-Hg protons in  $3^\circ$  amine ( $\text{R}_3\text{N}$ ) appeared at 3.15 ppm

The  $^1\text{H}$  NMR spectrum of quaternized  $\kappa$ -c was shown in figure 15c-15f. The presence of q188 on the  $\kappa$ -c back bone was confirmed by the appearance of signal at

3.15 ppm, which corresponded to the methyl groups linked to the quaternary nitrogen in the substituent of q188. [23, 24] Further,  $^1\text{H}$  NMR analysis indicated the %DQ of quaternized as 10, 25, 50 and 75 % (v/v) q188- $\kappa$ -c to be 1.20, 2.1, 2.12. and 2.12% DQ, respectively.

Thus, we may be selected 25% (v/v) q188- $\kappa$ -c concentration because of its shows highs of %DQ. That can be concluded success that to the quaternization of  $\kappa$ -c by 25% (v/v) q188.

The  $^1\text{H}$  NMR spectra of q188- $\kappa$ -c were observed the Ha-Hg protons of q188 on  $\kappa$ -c back bone as shown in Figure 16c-16f. showed the Specific peaks of q188 at 3.15 ppm appeared and  $\kappa$ -c at 3.50-4.00 and 5.25 ppm appeared [25]. Furthermore, the DS, as calculated from eq (4) using integration areas from  $^1\text{H}$  NMR spectra was 2.1%DQ



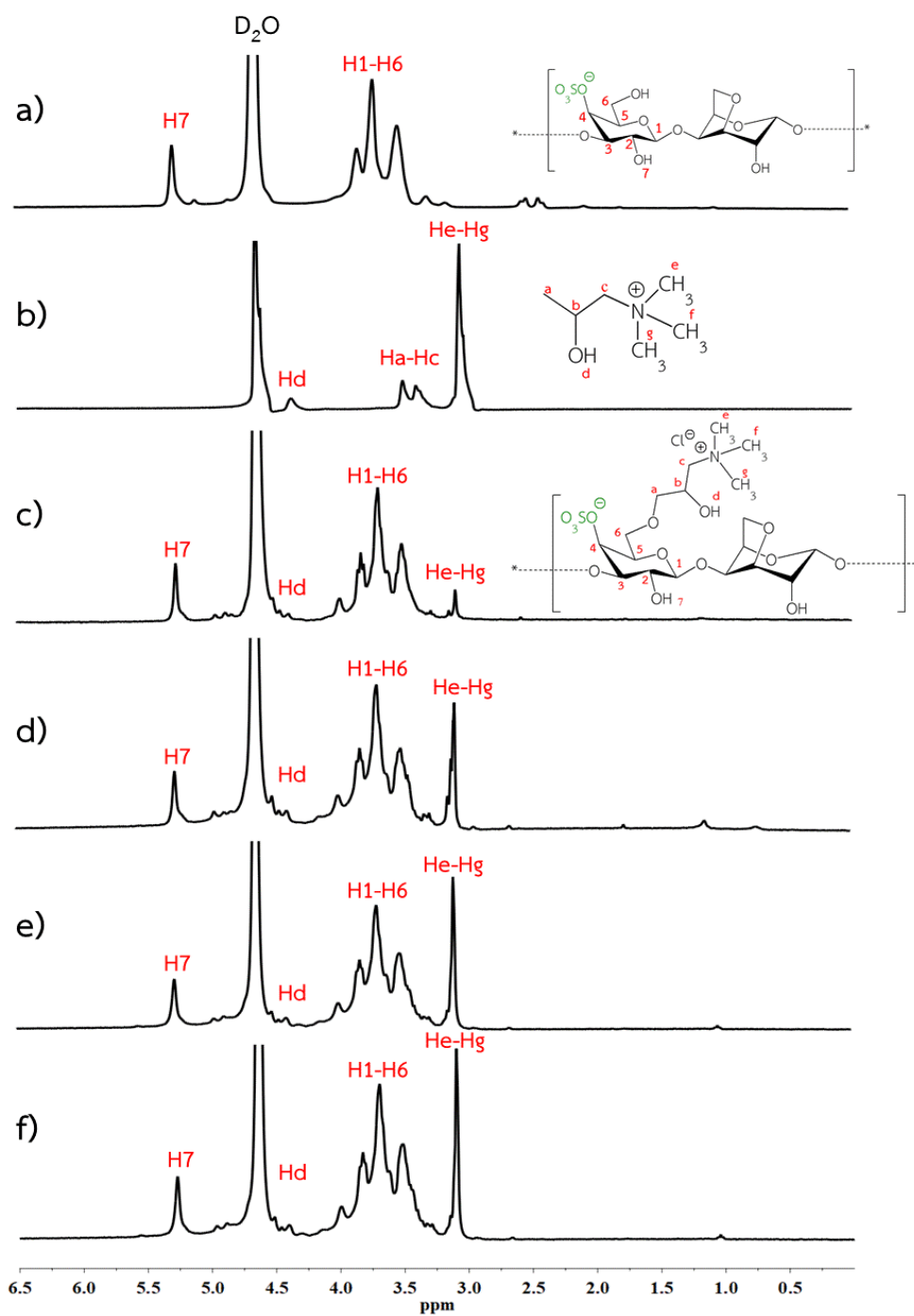


**Figure 15**  $^1\text{H}$  NMR spectra of (a)  $\kappa$ -c, (b) q188, (c-f) 10, 25, 50, 75 % (v/v) q188- $\kappa$ -c used as various concentrations, respectively



## 4.2 Swelling Controlled Release

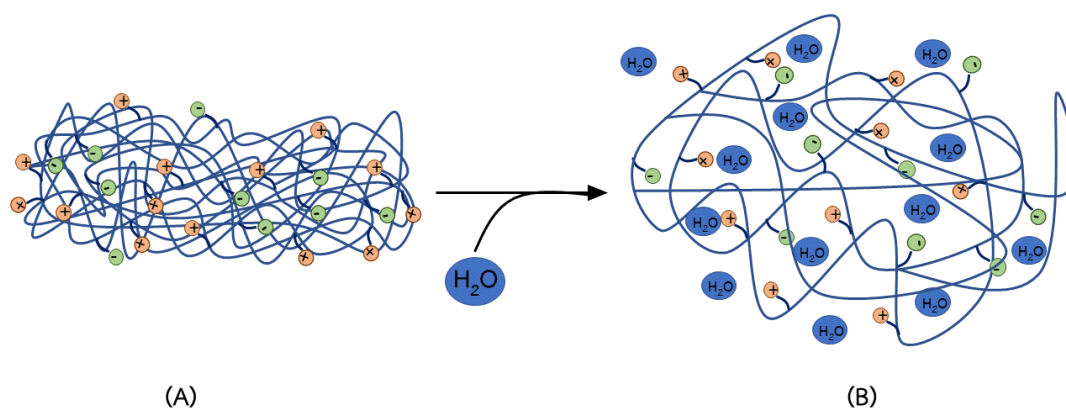


**Figure 16** Presentation of swelling controlled release[2]

4.2.1 The solubility of  $\kappa$ -c and q188- $\kappa$ -c with PBS for pH 7.4

The Modified of 10, 25, 50 and 75% (v/v) q188- $\kappa$ -c can be increase solubility because of its  $11.4 \pm 0.04$ ,  $43.7 \pm 0.01$ ,  $69.0 \pm 0.02$  and  $69.3 \pm 0.01$ % solubility, respectively to higher than that unmodified of  $\kappa$ -c which presented  $7.24 \pm 2.85$ % solubility. Thus, A high concentration of q188 can be promote solubility.

**Table 3** The solubility studied of synthesize of q188- $\kappa$ -c with difference concentration of q188

Concentrations of q188 (% v/v)	Solubility (%)
$\kappa$ -c	$7.24 \pm 2.85$
10	$11.4 \pm 0.04$
25	$43.7 \pm 0.01$
50	$69.0 \pm 0.02$
75	$69.3 \pm 0.01$

## 4.3 Zeta-potential analysis

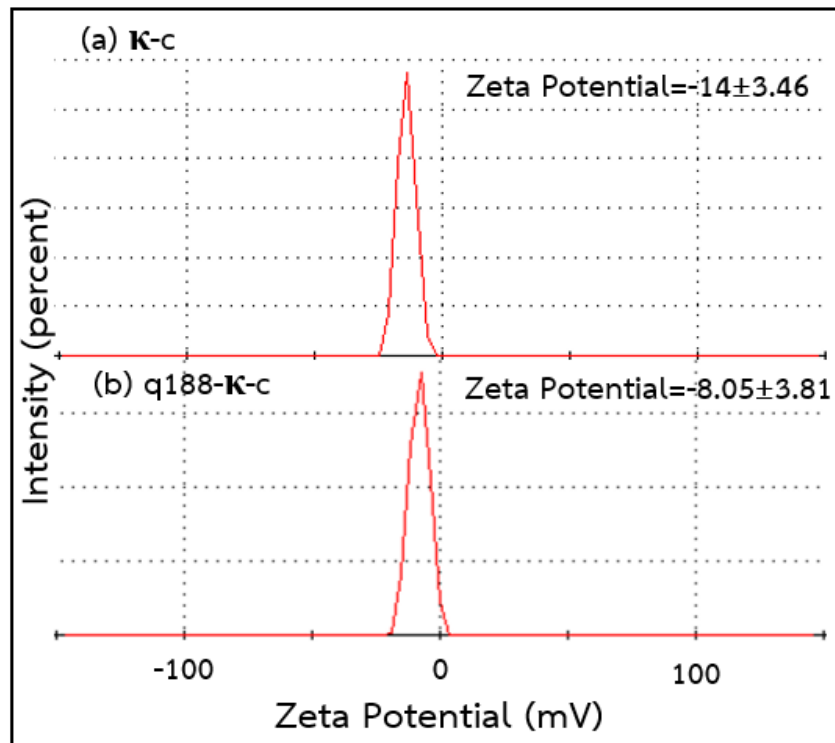


**Figure 17** Zeta-potential analysis of (a)  $\kappa$ -c and (b) q188- $\kappa$ -c derivatives as a modified to charge.

We measured the zeta-potential of  $\kappa$ -c and q188- $\kappa$ -c as shown in Figure.17, which studied of the effect positive charge from q188 on  $\kappa$ -c backbone. the Zeta-potential value of  $\kappa$ -c and q188- $\kappa$ -c were  $-14 \pm 3.46$  and  $-8.05 \pm 3.81$  mV, respectively. This increase of zeta-potential value is probably due to the positive charge of q188 and suggests that quaternization q188 can be enhanced positives charge onto  $\kappa$ -c backbone. The positive charge can be increase interaction with negative charge of skin. Thus, to enhanced positive charge of q188- $\kappa$ -c can be increase electrostatic interaction with cell membrane for transdermal delivery systems.

## Part II: The preparation and characterization of q188-κ-c and its derivatives used as reducing and stabilizer agent for synthesis of AuNPs.

### 4.4 The synthesis of q188-κ-c@AuNPs

The efficient and rapid synthesis for controlling the morphology, shape and size distribution of suitable q188-κ-c@AuNPs derivatives under optimal condition (1mM HAuCl<sub>4</sub> solution, 25%(v/v) q188-κ-c at 70°C for 1h., pH 7) for anti-inflammatory drug and cancer drug delivery systems were characterized by UV-vis, TEM, Zeta potential and EDS. In this research, q188-κ-c@AuNPs was successfully reduction of HAuCl<sub>4</sub> with 25% (v/v) q188-κ-c as stabilizing and reducing.[26].

#### 4.4.1 Ultraviolet-visible (UV-vis) spectroscopy

In the present study, we interested to use the reducing and stabilizing nature of biopolymer, q188-κ-c for the synthesis of gold nanoparticles as shown in Figure.18. The different colors of AuNPs were different morphologies appear. Hence, AuNPs were monitored with the color change and UV-vis spectroscopy. In addition, the effects of q188-κ-c concentrations as a reducing and stabilizing agent that studied based on ability to control the morphology and size of AuNPs. Thus, q188-κ-c was stabilized gold nanoparticles (q188-κ-c@AuNPs) allowed the attachment of a large number of small molecules which will exclusively target the inflammatory cells and cancer cells.

The initial synthesis of AuNPs was carried out in a synthesis containing q188-κ-c, κ-c mixed NaOH and distilled water. The synthesis of κ-c was added q188 with various concentration of q188. Then, HAuCl<sub>4</sub> was added into the mixture in hot water. The color change was occurred from colorless to red colored suspension. The absorbance was measured on UV-visible spectrophotometer.

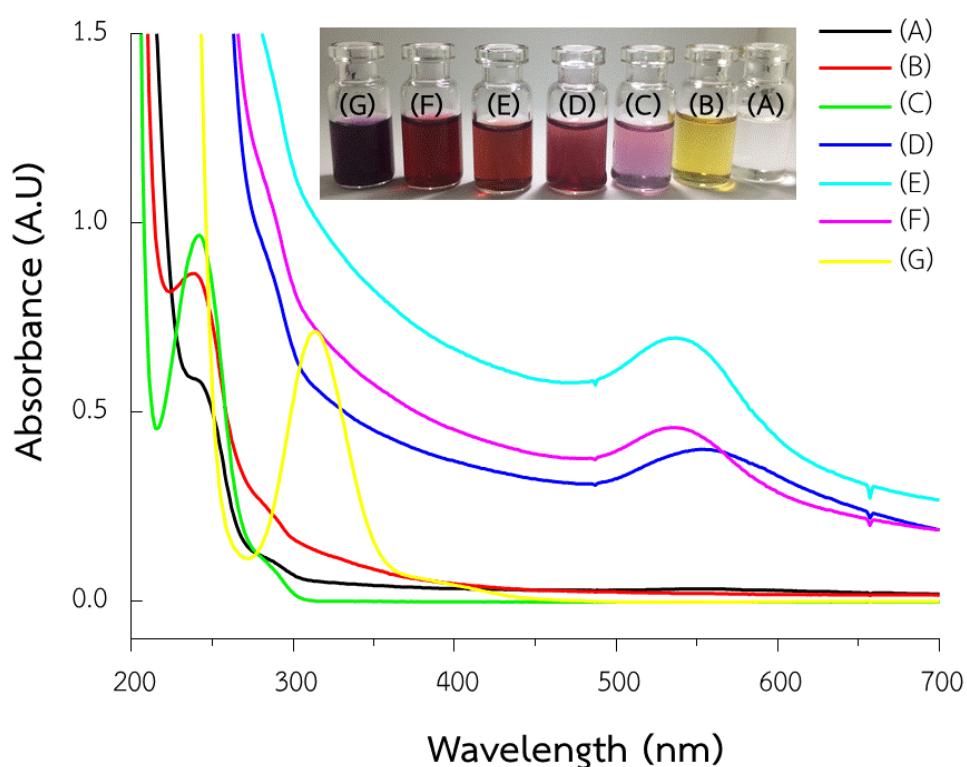


**Figure 18** The absorption spectra of q188- $\kappa$ -c@AuNPs were measured at wavelength range of 200-700 nm on microtiter plate reader; (A) pure  $\kappa$ -c, (B) solution of  $\text{HAuCl}_4$ , (C) 1% (w/v)  $\kappa$ -c with  $\text{HAuCl}_4$  solution, (D) 10% (v/v) q188- $\kappa$ -c@AuNPs, (E) 25% (v/v) q188- $\kappa$ -c@AuNPs, (F) 50% (v/v) q188- $\kappa$ -c@AuNPs and (G) 75% (v/v) q188- $\kappa$ -c@AuNPs

The UV-vis spectra showed the absorption peaks in Figure.18. We synthesized AuNPs using various concentration of q188 from 10 % (v/v) to 75% (v/v) with 1% (w/v)  $\kappa$ -c for reduced and stabilized of 1 mM  $\text{HAuCl}_4$  solution. The q188- $\kappa$ -c@AuNPs at 25% (v/v) q188- $\kappa$ -c, was the optimum condition with the maximum absorption that higher than other conditions and wavelength average is 530 nm and finally, the color of solution turned to red (showed in Figure.18E and Figure.18F). The spectra 25% (v/v) and 50% (v/v) q188- $\kappa$ -c have a strong absorption feature at 530 nm due to the characteristic surface plasmon resonance of AuNPs [27]. Thus, the condition 25% (v/v)

and 50% (v/v) q188- $\kappa$ -c used as a reducer and stabilizer of AuNPs, which studied on aggregation of AuNPs.

#### 4.4.2 Aggregation of gold Nanoparticles (AuNPs)

The different colors from red-wine to violet color were shown aggregation of AuNPs because of SPR effect.

The synthesized of 25% (v/v) q188- $\kappa$ -c@AuNPs and 50% (v/v) q188- $\kappa$ -c@AuNPs were keep 25% (v/v) q188- $\kappa$ -c@AuNPs and 50% (v/v) q188- $\kappa$ -c@AuNPs at room temperature for a week. The aggregation was observed by UV-vis spectrophotometer that showed in Figure 19.

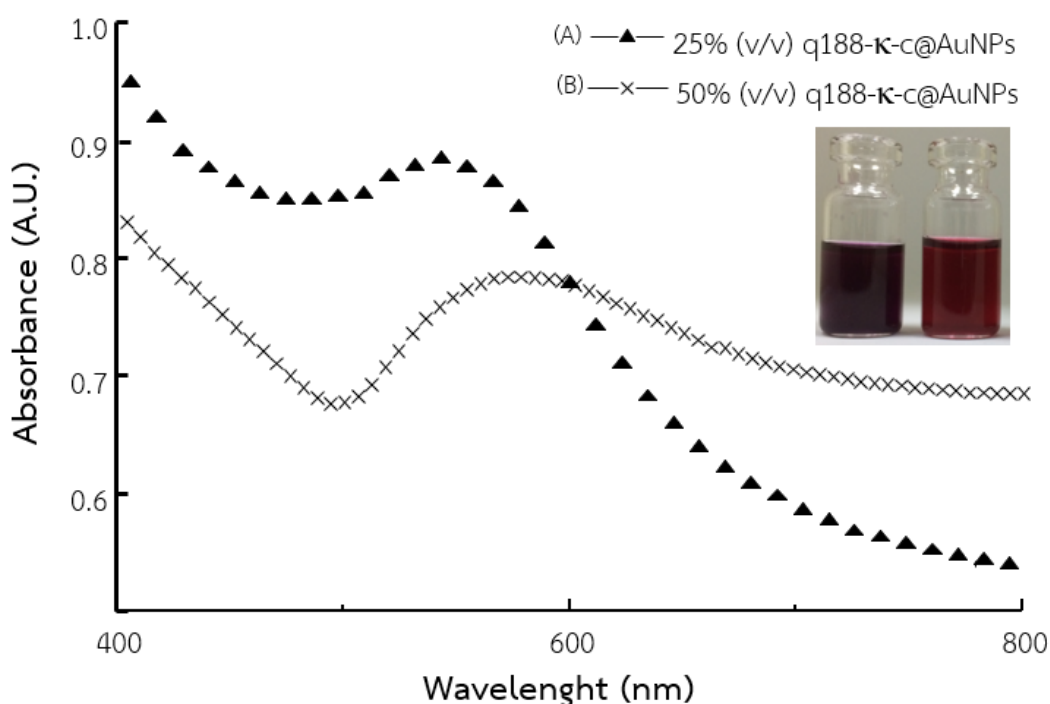


**Figure 19** The absorption spectra of q188- $\kappa$ -c@AuNPs were measured at wavelength range of 400-800 nm on microtiter plate reader; (A) 25% (v/v) q188- $\kappa$ -c@AuNPs, (B) 50% (v/v) q188- $\kappa$ -c@AuNPs.

The synthesized 50% (v/v) q188- $\kappa$ -c was shown aggregation. Thus, 25% (v/v) q188- $\kappa$ -c condition was the optimum condition that its high stability. [27]

#### 4.4.2 FT-IR spectroscopy (ATR mode) analysis

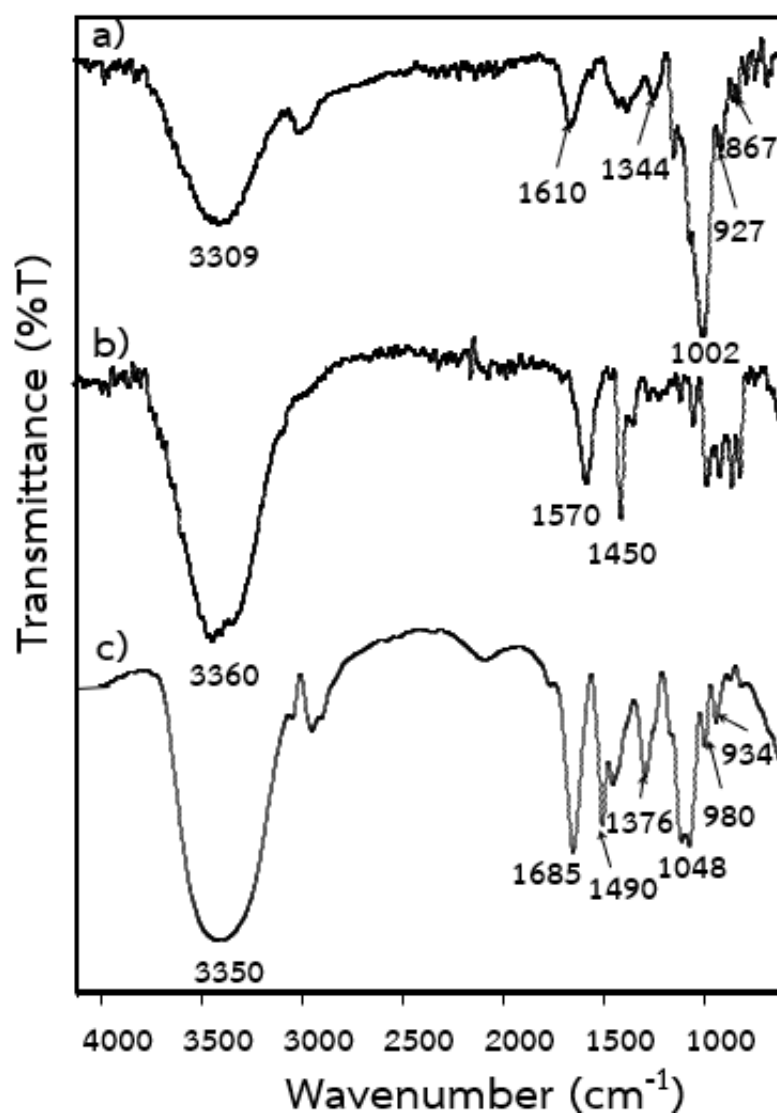


**Figure 20** FT-IR spectra of (a)  $\kappa$ -c, (b) q188, (c) 25% (v/v) q188- $\kappa$ -c used as various concentrations.

The  $\kappa$ -c, q188 and q188- $\kappa$ -c derivatives were characterized by FT-IR analysis. FT-IR spectrum of  $\kappa$ -c, q188 and q188- $\kappa$ -c are shown in Figure. 20. The FT-IR spectra of the unmodified  $\kappa$ -c and modified of  $\kappa$ -c on back bone were shown in Figure.20a. and

Figure 20c, respectively. The spectrum of the  $\kappa$ -c without as a quaternization of q188 (Figure. 20a) showed a strong broad band at  $3309\text{ cm}^{-1}$ , which corresponded to the O–H stretching. The presence of two signals at  $867$  and  $927\text{ cm}^{-1}$  was assigned to R–O–S– stretching vibration of galactose residue. The characteristic  $\kappa$ -c peak belonging to the R–O–SO<sub>3</sub> stretching of the D-galactose-4-sulfate residue was observed at  $1002$  and  $1344\text{ cm}^{-1}$ . The FT-IR spectrum of q188 in Figure. 20b reveals that the broad band at  $3360\text{ cm}^{-1}$  was of an O–H stretching. The band at  $1570\text{ cm}^{-1}$  was assigned to the –CH<sub>3</sub> stretching. The band at  $1450\text{ cm}^{-1}$  was due to the N–C stretching adsorption band. After quaternization of  $\kappa$ -c (q188- $\kappa$ -c), the FT-IR spectrum of q188- $\kappa$ -c (Figure. 20c) showed a peak shift at  $1048$  and  $1376\text{ cm}^{-1}$  corresponding to the R–O–S– stretching vibration of galactose residue, a band shift at  $1490\text{ cm}^{-1}$  that N–C stretching in the methyl groups, and band to shift at  $934$  and  $980\text{ cm}^{-1}$  that was assigned to the asymmetric stretching of R–O–SO<sub>3</sub> of the D-galactose-4-sulfate residue of  $\kappa$ -c. Thus, the results demonstrated that, confirm of q188- $\kappa$ -c derivatives was successfully quaternized on  $\kappa$ -c back bone.

#### 4.4.3 Dynamic light scattering (DLS)

In this work studied in control of average particles size and narrow size distribution that important to use nanoparticles in many applications. The size distributions of q188- $\kappa$ -c@AuNPs can observed by DLS. In the absence of q188- $\kappa$ -c@AuNPs shown in table 4

**Table 4** The size distribution of q188- $\kappa$ -c@AuNPs derivatives and q188- $\kappa$ -c@Pur@AuNPs.

Compound	Size (nm)
q188- $\kappa$ -c@AuNPs	100
q188- $\kappa$ -c@Pur@AuNPs	170

The TEM images recorded from as synthesized AuNPs (Figure 21) revealed that the nanoparticles were well dispersed with a narrow size distribution and an average size of 15 nm (Figure 21a-d). The morphology of q188- $\kappa$ -c@AuNPs was the spherical shape. In subsequent experiments, Therefore, q188- $\kappa$ -c@AuNPs was drug carrier as a prepare of drug loading.

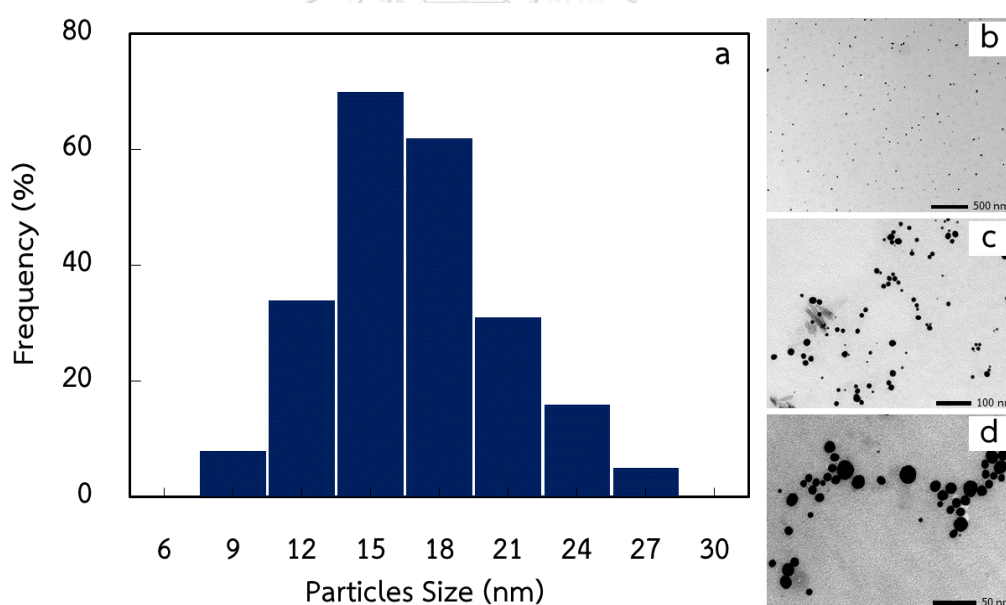


**Figure 21** The morphology of q188- $\kappa$ -c@AuNPs a) the particle size of q188- $\kappa$ -c@AuNPs from histogram, b-d) the sphere and particle sized of q188- $\kappa$ -c@AuNPs.



#### 4.4.5 Energy Dispersive X-ray Spectrometry (EDX)

The spot profile EDX spectrum and TEM image recorded from the AuNPs are shown in Figure. 22. The EDX profile was shown a strong gold signal along with weak oxygen and strong carbon peaks, which may have originated from the biomolecules that were bound to the surface of the AuNPs. The TEM image was shown the spherical shape of AuNPs and an average size of 15 nm.

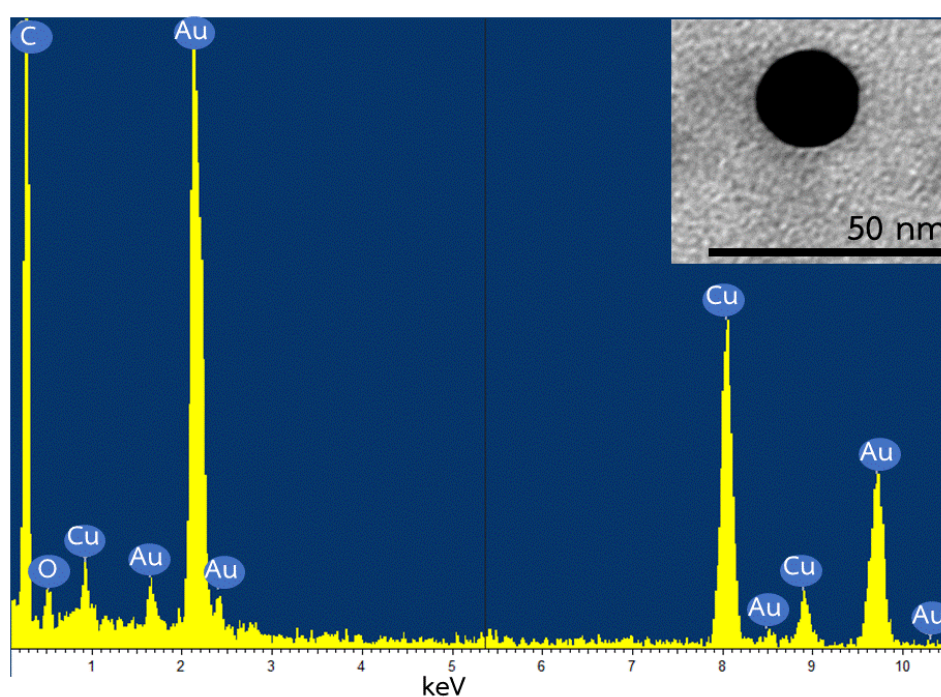


**Figure 22** Characterization of the gold nanoparticles formed by the reaction of 25% (v/v) q188-κ-c@AuNP: Spot profile EDX spectrum.

**Part III: The Preparation and preliminary were cytotoxic studied of Pur load on q188-κ-c@AuNPs derivatives for evaluation of biological activity.**

4.5 The synthesis of q188-κ-c@Pur@AuNPs

4.5.1 FT-IR spectroscopy (ATR mode)

In 25% (v/v) q188-κ-c@AuNPs, the characteristic absorption peaks at  $1450\text{ cm}^{-1}$  was due to the N–C stretching absorption band. After quaternization of κ-c (q188-κ-c), the FT-IR spectrum of q188-κ-c (Figure. 23a) showed a peak shift at  $1048$  and  $1376\text{ cm}^{-1}$  corresponding to the R–O–S stretching vibration of galactose residue, a band shift at  $1490\text{ cm}^{-1}$  that N–C stretching in the methyl groups, and band to shift at  $934$  and  $980\text{ cm}^{-1}$  that was assigned to the asymmetric stretching of R–O–SO<sub>3</sub> of the D-galactose-4-sulfate residue of κ-c.

In pure puerarin (Figure.23b), the characteristic absorption peaks at  $3331\text{ cm}^{-1}$  due to O–H stretching of sugar,  $2750\text{ cm}^{-1}$  due to symmetric stretching vibration of –CH<sub>3</sub>.  $1603\text{ cm}^{-1}$ , an absorption band at  $1650$  and  $1515\text{ cm}^{-1}$  due to stretching vibration from –COOH stretching and –CO stretching in aromatic of sugar, respectively. [28].

The FT-IR spectra of 25% (v/v) q188-κ-c@Pur@AuNPs (Figure 23C). was displayed an absorption band at  $1273$  and  $1059\text{ cm}^{-1}$  corresponding to the R–O–S stretching vibration of galactose residue, an absorption band shift at  $1517\text{ cm}^{-1}$  that N–C stretching in the methyl groups, and band to shift at  $937$  and  $985\text{ cm}^{-1}$  that was assigned to the asymmetric stretching of R–O–SO<sub>3</sub> of the D-galactose-4-sulfate residue of κ-c, an absorption band at  $1670$  and  $1650\text{ cm}^{-1}$  due to stretching vibration from –COOH stretching and –CO stretching from sugar of puerarin, respectively. Thus, the results demonstrated that confirmed of puerarin was successfully synthesis on 25% (v/v) q188-κ-c@AuNPs derivatives.

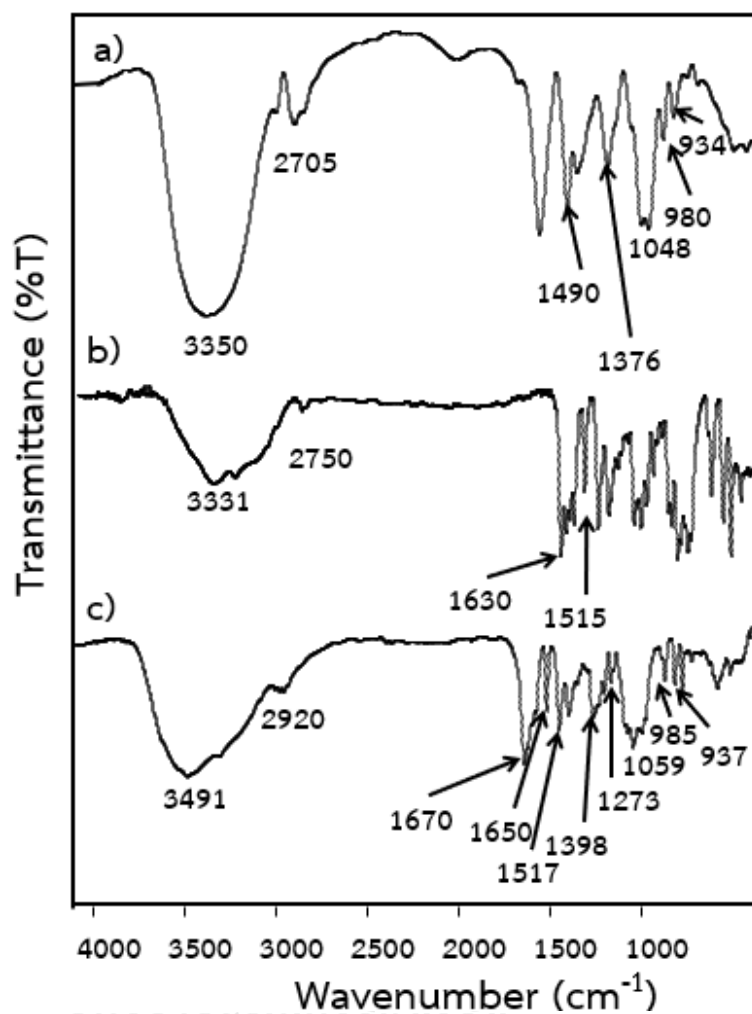


**Figure 23** FT-IR spectra of: (a) 25% (v/v) q188- $\kappa$ -c@AuNPs, (b) Puerarin and 25% (v/v) q188- $\kappa$ -c@Pur@AuNPs.

#### 4.6 Biological activities of q188-κ-c@Pur@AuNPs with cancer and inflammatory cell

line.

##### 4.6.1 Cytotoxicity study of q188-κ-c@Pur@AuNPs

To study enhanced cytotoxicity and intracellular uptake, we studied anti-cancer and anti-inflammatory activities of q188-κ-c@Pur@AuNPs as bio-nanocarriers and as an active targeted nanocarriers. The firstly study to evaluate their cytotoxicity of q188-κ-c@Pur@AuNPs using MTT assay against human cancer cell, human inflammatory cell and normal cell such as KATO III (stomach carcinoma), Chago-K1 (lung carcinoma), SW 620 (colon carcinoma), CLS (oral cancers) and RAW 264.7 (inflammatory cell) and normal cell (Wi-38).

The platform of Pur, q188-κ-c@AuNPs, q188-κ-c@Pur@AuNPs and diclofenac were showed different cytotoxic activities in each cancer cells. Among these, q188-κ-c@Pur@AuNPs exhibited high cytotoxic activity against CLS with  $IC_{50}$  of  $5.06 \pm 0.05$  more sensitive than Pur alone and diclofenac with  $IC_{50}$  of  $50.91 \pm 0.05$  and  $5.66 \pm 1.84$ , respectively (Table 5).

**Table 5** *In vitro* cytotoxic of compound against CLS, SW 620, Chago-K1, KATO III and RAW 26.7.

Compounds	Cytotoxic ( $IC_{50}$ , $\mu$ M)				
	CLS	SW 620	Chago-K1	KATO III	RAW 264.7
Pur	$50.91 \pm 0.05$	$56.45 \pm 0.05$	$56.44 \pm 0.63$	$26.29 \pm 0.05$	$36.35 \pm 1.10$
q188-κ-c@AuNPs	$26.09 \pm 0.15$	$5.26 \pm 1.66$	$5.39 \pm 1.18$	$6.66 \pm 0.03$	$3.93 \pm 2.53$
q188-κ-c@Pur@AuNPs	$5.06 \pm 0.05$	$3.33 \pm 0.04$	$2.24 \pm 1.07$	$26.29 \pm 0.05$	$2.69 \pm 0.76$
Diclofenac	$5.66 \pm 1.84$	$12.61 \pm 0.01$	$33.72 \pm 13.98$	$25.53 \pm 0.05$	$0.38 \pm 0.05$

#### 4.7 In vitro study of synthesise of q188-κ-c@Pur@AuNPs permeation through cellulose membrane by Franz's cell diffusion method

In vitro study of q188-κ-c@Pur@AuNPs permeation to cellulose acetate membrane by Franz's cell diffusion method was carried out in phosphate buffer saline (PBS) pH 7.4 for  $37 \pm 1^\circ\text{C}$ . The in vitro release profiles of amount of Pur and  $\text{Au}^0$  permeation from q188-κ-c@Pur@AuNPs compare with κ-c@Pur@AuNPs and κ-c@AuNPs per unit area were investigated for 6 hours which a characterization by Ultraviolet-visible spectroscopy (UV-vis spectroscopy) and Inductively Coupled Plasma Optical Emission Spectrometry (ICP-OES).

The permeation of Pur and  $\text{Au}^0$  from each compound was calculated in term of mean cumulative amount of permeated Pur and  $\text{Au}^0$  across a unit area of membrane with time which cumulative amount of permeated through a unit area of membrane ( $Q_p$ ) can be expressed using equation (7) as followed:

$$Q_p = \frac{CLC \times VB}{AM} \quad (7)$$

Here, CLC is concentration ( $\mu\text{g/ml}$ ) of Pur and  $\text{Au}^0$  across a unit area of membrane, VB is volume of PBS (mL) and AM is area of cellulose acetate membrane.

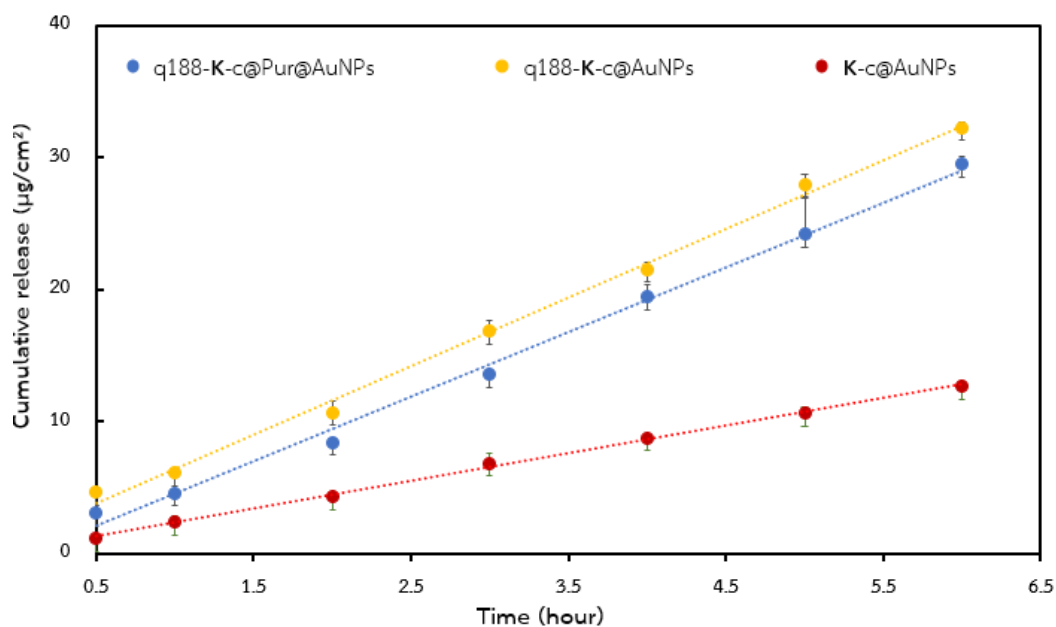


**Figure 24** Cumulative release of  $\text{Au}^0$  from q188- $\kappa$ -c@Pur@AuNPs compare with q188- $\kappa$ -c@AuNPs and  $\kappa$ -c@AuNPs permeating through one area division of cellulose membrane with different times.

The cumulative release profiles of  $\text{Au}^0$  from q188- $\kappa$ -c@Pur@AuNPs, q188- $\kappa$ -c@AuNPs and  $\kappa$ -c@AuNPs were shown increased continuously with time (Table 6 and Figure 25). Accordingly, the permeation behaviors of  $\text{Au}^0$  from q188- $\kappa$ -c@Pur@AuNPs, q188- $\kappa$ -c@AuNPs and  $\kappa$ -c@AuNPs were exhibited linear relationship from the straight-line portion of curve which slope of the linear correlation between cumulative amount of drug ( $Q_p$ ) and time as flux of  $\text{Au}^0$  ( $\mu\text{g}/\text{cm}^2\cdot\text{h}$ ) was shown in Figure. 24 and Table 9.

**Table 6** Flux relation of Au<sup>0</sup> in q188-κ-c@Pur@AuNPs compare with q188-κ-c@AuNPs and κ-c@AuNPs permeating through one area division of cellulose membrane and times.

Time (hour)	Flux (μg/cm <sup>2</sup> .h.)		
	q188-κ-c@Pur@AuNPs	q188-κ-c@AuNPs	κ-c@AuNPs
0.5	3.04	4.67	1.09
1	4.58	6.08	2.90
2	8.42	10.68	4.33
3	13.53	16.81	6.85
4	19.40	21.53	8.76
5	24.18	27.93	10.61
6	29.48	32.28	12.66
<b>Total (%)</b>	<b>52.1</b>	<b>60.40</b>	<b>23.7</b>

Flux relation of Au<sup>0</sup> and Pur were calculated from an according standard curve showed in Figure. 28.

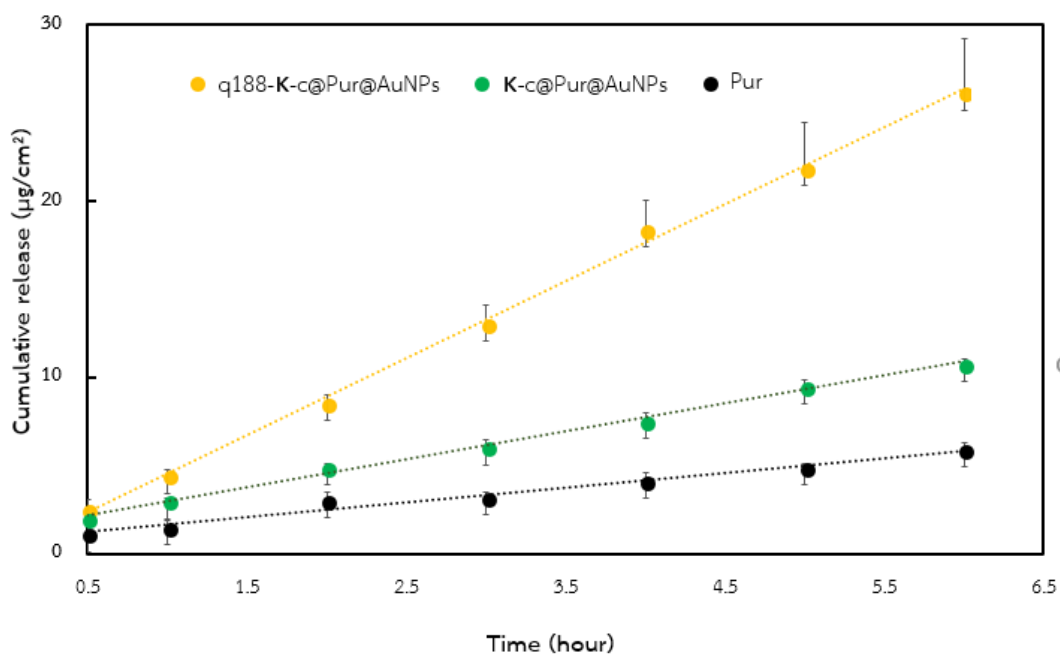


**Figure 25** Cumulative release of Pur in q188-κ-c@Pur@AuNPs compare with κ-c@Pur@AuNPs and Pur permeating through one area division of cellulose membrane with different times.

The cumulative release profiles of Pur within the obtained q188-κ-c@Pur@AuNPs compare with κ-c@Pur@AuNPs and pure of Pur were shown increased continuously with time (Table 7 and Figure 25). Accordingly, the permeation behaviors of Pur from q188-κ-c@Pur@AuNPs and κ-c@Pur@AuNPs were exhibited linear relationship from the straight-line portion of curve which slope of the linear correlation between cumulative amount of drug ( $Q_p$ ) and time as flux of Au<sup>0</sup> ( $\mu\text{g}/\text{cm}^2\cdot\text{h}$ ) was shown in Table 10.



**Table 7** Flux relation of Pur in q188-κ-c@Pur@AuNPs compare with κ-c@Pur@AuNPs and pure of Pur permeating through one area division of cellulose membrane and times.

Time (hour)	Flux ( $\mu\text{g}/\text{cm}^2\cdot\text{h}$ )		
	q188-κ-c@Pur@AuNPs	q188-κ-c@AuNPs	κ-c@AuNPs
0.5	2.52	1.99	1.14
1	4.44	3.01	1.55
2	8.55	4.91	3.02
3	13.07	6.06	63.22
4	18.44	7.54	4.13
5	21.87	9.52	4.89
6	26.18	10.79	5.94
<b>Total (%)</b>	<b>48</b>	<b>21.9</b>	<b>11.9</b>

The permeating fluxes were presented high value of Pur and Au<sup>0</sup> in q188-κ-c@Pur@AuNPs than κ-c@Pur@AuNPs and alone Pur, that the synthesized of q188-κ-c@AuNPs can be enhance transdermal delivery showed in Table 8.

**Table 8** %Flux relation of each compound was permeating through one area division of cellulose membrane.

Compound	%Flux (μg/cm <sup>2</sup> .h.)	
	Pur	Au <sup>0</sup>
q188-κ-c@Pur@AuNPs <sup>a</sup>	-	52
q188-κ-c@AuNPs <sup>a</sup>	-	60
κ-c@AuNPs <sup>a</sup>	-	24
q188-κ-c@Pur@AuNPs <sup>b</sup>	48	-
κ-c@Pur@AuNPs <sup>b</sup>	22	-
Pur <sup>b</sup>	12	-

Compound<sup>a</sup>: %Flux relation from ICP-OES.

Compound<sup>b</sup>: %Flux relation from UV-vis.

## CHAPTER V

### CONCLUSION

In conclusion, the nanoparticles for drug carriers have been used to improve insolubility of drug and enhance permeation through cell membrane

The modified of  $\kappa$ -c was successfully achieved via quaternization process.  $^1\text{H}$  NMR analysis indicated the %DQ of 25% (v/v) q188- $\kappa$ -c to be 21%. Also explored was solubility with pH 7.4 buffer, the synthesized of 25% (v/v) q188- $\kappa$ -c  $43.7 \pm 0.01\%$  solubility and high stable more than that unmodified which presented  $11 \pm 0.03\%$  solubility. The preparation AuNPs used as reducing and stabilizing of q188- $\kappa$ -c (q188- $\kappa$ -c@AuNPs) which showed sphere of shape and sized at 15 nm and 100 nm by TEM and DLS characterized, respectively. The q188- $\kappa$ -c@Pur@AuNPs derivatives used as to preparation by load on q188- $\kappa$ -c@AuNPs derivative that showed size at 25 nm and 170 nm by TEM and DLS characterized, respectively. The preliminary study of cytotoxicity was non-cytotoxic to human normal cells (Wi-38) and enhanced activities of q188- $\kappa$ -c@Pur@AuNPs against CLS cell with  $\text{IC}_{50}$   $5.06 \pm 0.05$   $\mu\text{M}$  that than alone Pur. *In vitro* study was drug permeation through cellulose membrane by Franz' cell diffusion that permeating fluxes were presented high value of q188- $\kappa$ -c@Pur@AuNPs than  $\kappa$ -c@Pur@AuNPs and alone Pur which confirm enhance transdermal delivery by ICP-OES and UV-vis spectrophotometer.

Thus, the synthesized of q188- $\kappa$ -c@Pur@AuNPs was high solubility, non-toxic with normal cell and increase activities with CLS cell which can be used as enhance permeation for transdermal delivery

## REFERENCES

- [1] De Jong, W.H. and Borm, P.J. Drug delivery and nanoparticles: applications and hazards. International journal of nanomedicine 3(2) (2008): 133.
- [2] Ajnai, G., Chiu, A., Kan, T., Cheng, C.-C., Tsai, T.-H., and Chang, J. Trends of gold nanoparticle-based drug delivery system in cancer therapy. Journal of Experimental & Clinical Medicine 6(6) (2014): 172-178.
- [3] Prajapati, V.D., Maheriya, P.M., Jani, G.K., and Solanki, H.K. RETRACTED: Carrageenan: A natural seaweed polysaccharide and its applications. Carbohydrate polymers 105 (2014): 97-112.
- [4] Li, L., Ni, R., Shao, Y., and Mao, S. Carrageenan and its applications in drug delivery. Carbohydrate polymers 103 (2014): 1-11.
- [5] Salgueiro, A.M., Daniel-da-Silva, A.L., Fateixa, S., and Trindade, T. K-Carrageenan hydrogel nanocomposites with release behavior mediated by morphological distinct Au nanofillers. Carbohydrate polymers 91(1) (2013): 100-109.
- [6] Huang, X. and El-Sayed, M.A. Gold nanoparticles: optical properties and implementations in cancer diagnosis and photothermal therapy. Journal of advanced research 1(1) (2010): 13-28.
- [7] Liu, X.-s., Jiang, J., Jiao, X.-y., Wu, Y.-e., Lin, J.-h., and Cai, Y.-m. Lycorine induces apoptosis and down-regulation of Mcl-1 in human leukemia cells. Cancer Letters 274(1) (2009): 16-24.
- [8] Pattison, D.J. and Winyard, P.G. Dietary antioxidants in inflammatory arthritis: do they have any role in etiology or therapy? Nat Clin Pract Rheum 4(11) (2008): 590-596.
- [9] BERENBAUM, F. Free radicals and inflammation. Annals of the Rheumatic Diseases 60(5) (2001): 442.
- [10] Frölich, L. and Riederer, P. Free radical mechanisms in dementia of Alzheimer type and the potential for antioxidative treatment. Arzneimittel-Forschung 45(3A) (1995): 443-446.

- [11] Elgorashi, E.E., Stafford, G.I., and van Staden, J. Acetylcholinesterase Enzyme Inhibitory Effects of Amaryllidaceae Alkaloids. Planta Med 70(03) (2004): 260-262.
- [12] Ghosh, P., Han, G., De, M., Kim, C.K., and Rotello, V.M. Gold nanoparticles in delivery applications. Advanced Drug Delivery Reviews 60(11) (2008): 1307-1315.
- [13] Hickey, T., Kreutzer, D., Burgess, D.J., and Moussy, F. Dexamethasone/PLGA microspheres for continuous delivery of an anti-inflammatory drug for implantable medical devices. Biomaterials 23(7) (2002): 1649-1656.
- [14] França, A., Aggarwal, P., Barsov, E.V., Kozlov, S.V., Dobrovolskaia, M.A., and González-Fernández, Á. Macrophage scavenger receptor A mediates the uptake of gold colloids by macrophages in vitro. Nanomedicine 6(7) (2011): 1175-1188.
- [15] Chen, H., Dorrigan, A., Saad, S., Hare, D.J., Cortie, M.B., and Valenzuela, S.M. In Vivo Study of Spherical Gold Nanoparticles: Inflammatory Effects and Distribution in Mice. PLoS ONE 8(2) (2013): e58208.
- [16] Sumbayev, V.V., et al. Gold Nanoparticles Downregulate Interleukin-1 $\beta$ -Induced Pro-Inflammatory Responses. Small 9(3) (2013): 472-477.
- [17] Karande, P. and Mitragotri, S. Enhancement of transdermal drug delivery via synergistic action of chemicals. Biochimica et Biophysica Acta (BBA) - Biomembranes 1788(11) (2009): 2362-2373.
- [18] Chien, Y.W., Keshary, P.R., Huang, Y.C., and Sarpotdar, P.P. Comparative controlled skin permeation of nitroglycerin from marketed transdermal delivery systems. Journal of pharmaceutical sciences 72(8) (1983): 968-970.
- [19] Yang, Y., et al. Inhibition of nitric oxide synthesis delayed mature-green tomato fruits ripening induced by inhibition of ethylene. Scientia Horticulturae 211 (2016): 95-101.
- [20] Kim, H.K., Cheon, B.S., Kim, Y.H., Kim, S.Y., and Kim, H.P. Effects of naturally occurring flavonoids on nitric oxide production in the macrophage cell line RAW 264.7 and their structure-activity relationships. Biochem Pharmacol 58(5) (1999): 759-65.

- [21] Yang, E.-J., Yim, E.-Y., Song, G., Kim, G.-O., and Hyun, C.-G. Inhibition of nitric oxide production in lipopolysaccharide-activated RAW 264.7 macrophages by Jeju plant extracts. in *Interdisciplinary Toxicology*. 2009. 245.
- [22] Chivankul, T., Pengprecha, S., Padungros, P., Siraleartmukul, K., Prasongsuk, S., and Muangsin, N. Enhanced water-solubility and mucoadhesion of N,N,N-trimethyl-N-gluconate-N-homocysteine thiolactone chitosan. Carbohydrate Polymers 108 (2014): 224-231.
- [23] Selvakumaran, S., Muhamad, I.I., and Abd Razak, S.I. Evaluation of kappa carrageenan as potential carrier for floating drug delivery system: Effect of pore forming agents. Carbohydrate Polymers 135 (2016): 207-214.
- [24] Barahona, T., et al. Cationization of kappa- and iota-carrageenan – Characterization and properties of amphoteric polysaccharides. Carbohydrate Polymers 126 (2015): 70-77.
- [25] Lee, S.J., Shim, Y.-H., Oh, J.-S., Jeong, Y.-I., Park, I.-K., and Lee, H.C. Folic-acid-conjugated pullulan/poly(DL-lactide-co-glycolide) graft copolymer nanoparticles for folate-receptor-mediated drug delivery. Nanoscale Research Letters 10(1) (2015): 1-11.
- [26] Shankar, S.S., Rai, A., Ahmad, A., and Sastry, M. Rapid synthesis of Au, Ag, and bimetallic Au core–Ag shell nanoparticles using Neem (*Azadirachta indica*) leaf broth. Journal of Colloid and Interface Science 275(2) (2004): 496-502.
- [27] Dixit, V., Van den Bossche, J., Sherman, D.M., Thompson, D.H., and Andres, R.P. Synthesis and Grafting of Thiocytic Acid–PEG–Folate Conjugates onto Au Nanoparticles for Selective Targeting of Folate Receptor-Positive Tumor Cells. Bioconjugate Chemistry 17(3) (2006): 603-609.
- [28] Huang, H., Yuan, Q., Shah, J.S., and Misra, R.D. A new family of folate-decorated and carbon nanotube-mediated drug delivery system: synthesis and drug delivery response. Adv Drug Deliv Rev 63(14-15) (2011): 1332-9.



APPENDIX

จุฬาลงกรณ์มหาวิทยาลัย  
**CHULALONGKORN UNIVERSITY**

## APPENDIX (A)

In *vitro* study of drug permeation through cellulose membrane, presented of concentrations as  $\text{Au}^0$  by ICP-OES.

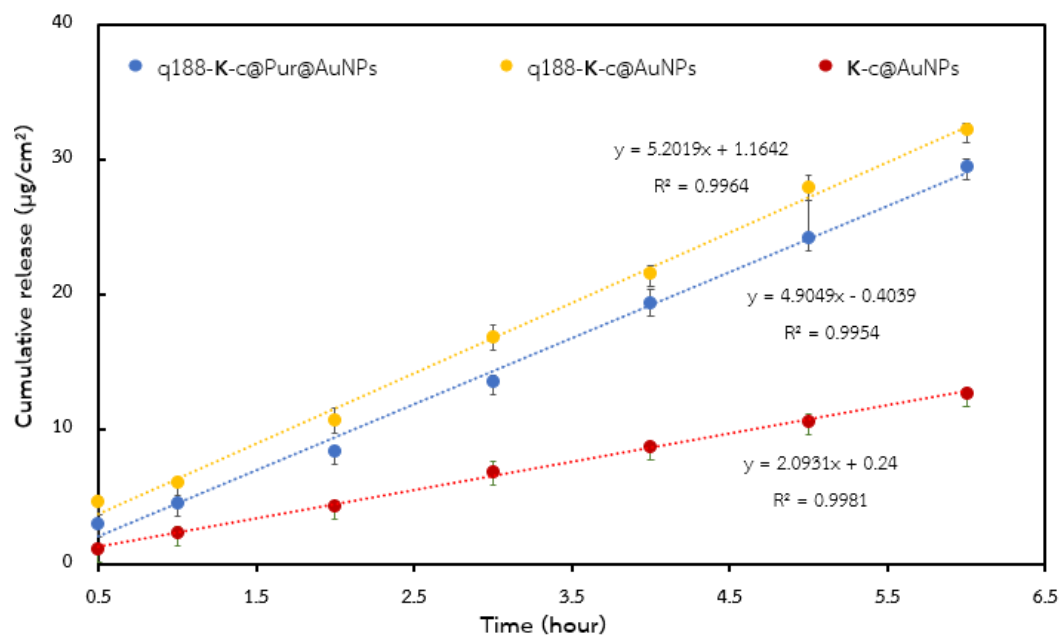


**Figure 26** Flux relation between amounts of q188-κ-c@Pur@AuNPs, q188-κ-c@AuNPs and κ-c@AuNPs permeating through one area division of cellulose membrane and times.

**Table 9** Flux relation between amounts of q188-κ-c@Pur@AuNPs, q188-κ-c@AuNPs and κ-c@AuNPs permeating through one area division of cellulose membrane and times.

Carrier	Linear relationship	r <sup>2</sup>	Flux (µg/cm <sup>2</sup> .hr)
q188-κ-c@Pur@AuNPs	$y = 5.2019x + 1.1642$	0.9964	5.20
q188-κ-c@AuNPs	$y = 4.9049x - 0.4039$	0.9954	4.90
κ-c @AuNPs	$y=2.0931x + 0.24$	0.9981	2.09



## APPENDIX (B)

In *vitro* study of drug permeation through cellulose membrane, presented of concentrations as Pur by UV-vis analysis.

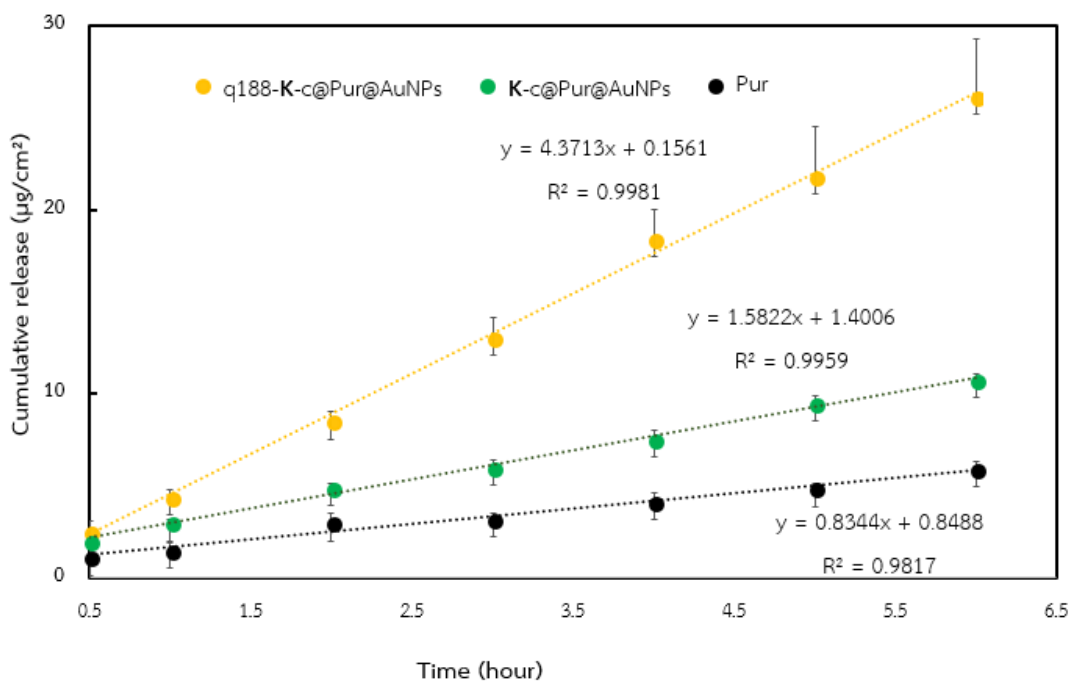


**Figure 27** Flux relation between amounts of q188-κ-c@Pur@AuNPs, κ-c@Pur@AuNPs and Pur permeating through one area division of cellulose membrane and times.

**Table 10** Flux relation between amounts of q188-κ-c@Pur@AuNPs, κ-c@Pur@AuNPs and Pur permeating through one area division of cellulose membrane and times.

Carrier	Linear relationship	r <sup>2</sup>	Flux (µg/cm <sup>2</sup> .hr)
q188-κ-c@Pur@AuNPs	$y = 4.3713x + 0.1561$	0.9981	4.3713
κ-c@Pur@AuNPs	$y = 1.5822x + 1.4006$	0.9959	4.9049
Pur	$y = 0.8344x + 0.8488$	0.9817	0.8344

## APPENDIX (D)

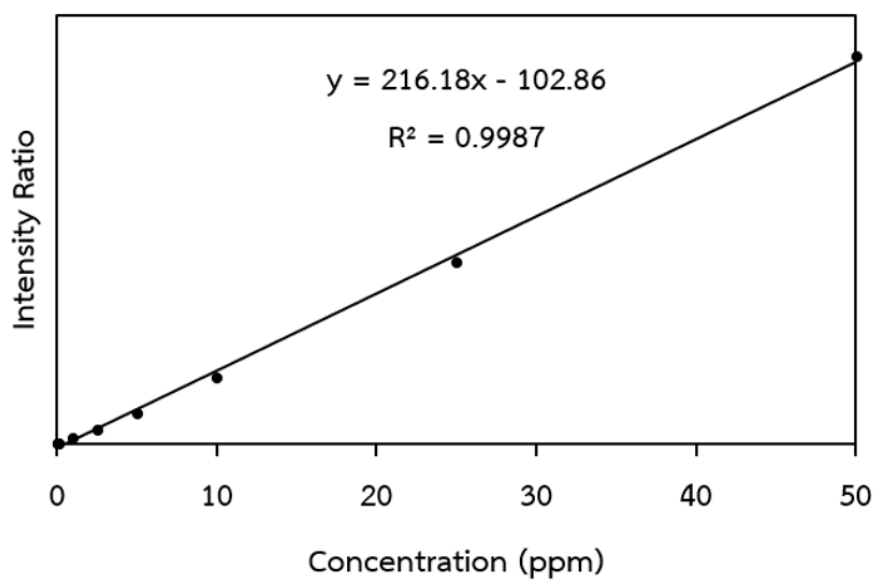


Figure 28 Calibration Curve of Au<sup>0</sup> from Franz's cell method by ICP-OES.

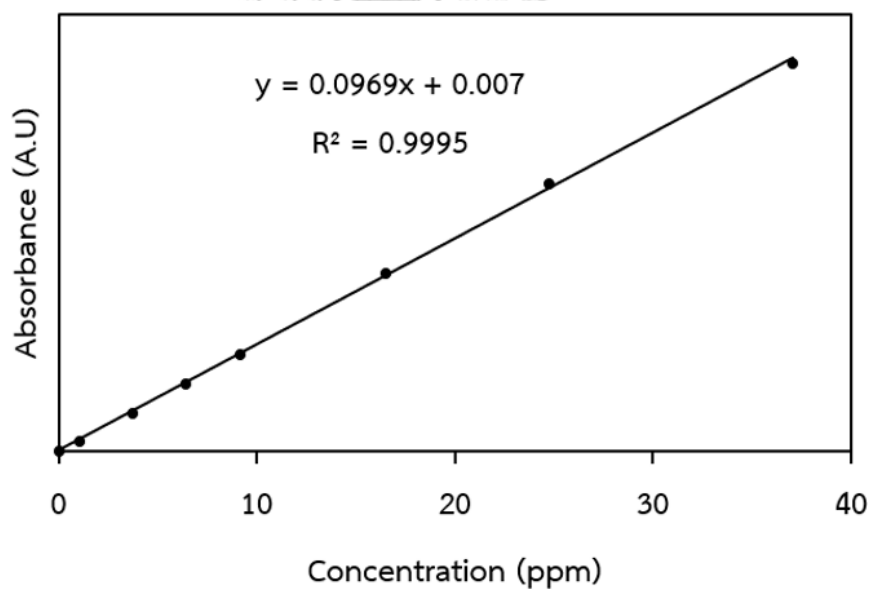


Figure 29 Calibration Curve of puerarin from Franz's cell method by UV-vis.

## VITA

Name: Ms. Kwanruen Chanpeng

Date of birth: April 28th, 1991

Nationality: Thai

Telephone: 0988307872

E-mail: Kwanruen\_ch91@hotmail.com

Address: 15 moo 7. Pafak, Phorncharoen, Bueng kan, 38180 Thailand.

Education:

- Master of Science (Petrochemistry and Polymer Science), Department of Petrochemistry and Polymer Science, Faculty of Science, Chulalongkorn University, Thailand, 2014-Present.
- Bachelor of Science (Chemistry), Department of Chemistry, Faculty of Science, Naresuan University, Thailand, 2010-2013.

Conference attendance:

- Kwanruen Chanpeng, Prof.Dr. Nongnuj Muengsin, on the topic of “Synthesis of puerarin-goldnanparticles for transdermal delivery”, Poster presentation at PPC & PETROMAT SYMPOSIUM 2017, Chulalongkorn University, Thailand.
- Kwanruen Chanpeng, Dr. Anusorn Warasing, on the topic of “Efficacy of the production of biodiesel from vegetable oil using heterogeneous catalyst from charcoal”, Poster presentation at Pure and Applied Chemistry International Conference 2013 (PACCON2013).